

Bayesian decomposition using Besov priors

A Horst¹, B M Afkham², Y Dong¹ and J Lemvig¹

¹ Department of applied mathematics and computer science, Technical university of Denmark, Matematiktorvet Kgs. Lyngby 2800, DK

² Research Unit of Mathematical Sciences, University of Oulu, Pentti Kaiteran katu 1, Linnanmaa, Finland

E-mail: ahor@dtu.dk

Abstract. In many inverse problems, the unknown is composed of multiple components with different regularities, for example, in imaging problems, where the unknown can have both rough and smooth features. We investigate linear Bayesian inverse problems, where the unknown consists of two components: one smooth and one piecewise constant. We model the unknown as a sum of two components and assign individual priors on each component to impose the assumed behavior. We propose and compare two prior models: (i) a combination of a Haar wavelet-based Besov prior and a smoothing Besov prior, and (ii) a hierarchical Gaussian prior on the gradient coupled with a smoothing Besov prior. To achieve a balanced reconstruction, we place hyperpriors on the prior parameters and jointly infer both the components and the hyperparameters. We propose Gibbs sampling schemes for posterior inference in both prior models. We demonstrate the capabilities of our approach on 1D and 2D deconvolution problems, where the unknown consists of smooth parts with jumps. The numerical results indicate that our methods improve the reconstruction quality compared to single-prior approaches and that the prior parameters can be successfully estimated to yield a balanced decomposition.

Keywords: Bayesian inference, Besov priors, decomposition, hierarchical models, Gibbs sampler.

1. Introduction

Inverse problems concern the estimation of unknown parameters of a system given indirect measurements. Such problems are typically ill-posed, meaning the computation of the solution is heavily sensitive to measurement limitations, measurement noise, and imprecise models. Stable solutions are often obtained through regularization techniques, which imposes penalties on the solution, e.g., periodicity, smoothness, nonsmoothness, or sparsity with respect to an expansion representation. In many inverse imaging problems the unknown parameters naturally consist of multiple components, e.g., image decomposition of cartoon and texture parts; see, for example, [1–5]. Taking the multiple components into account when modeling such inverse problems enables the use of a specific regularizer on each component to achieve a balanced solution that avoids overfitting to a subset of the components.

In this paper, we consider linear inverse problem with two components

$$\mathbf{y} = \mathbf{A}(\mathbf{g} + \mathbf{h}) + \epsilon, \quad \mathbf{f} = \mathbf{g} + \mathbf{h} \quad (1)$$

where $\mathbf{y} \in \mathbb{R}^m$ is the data, $\mathbf{f} \in \mathbb{R}^n$ is the unknown which is decomposed into the two components $\mathbf{g}, \mathbf{h} \in \mathbb{R}^n$, $\mathbf{A} \in \mathbb{R}^{m \times n}$ is the linear forward operator, and $\epsilon \in \mathbb{R}^m$ is additive noise. We assume that the component \mathbf{g} is piecewise constant and the component \mathbf{h} is smooth. These assumptions are reasonable in imaging applications such as anomaly detection in image deblurring [6, 7], atmospheric emission tomography [8], magnetoencephalography [9], and X-ray computed tomography [10].

Many variational methods have been proposed for signal or image decomposition [11–14], but all of these methods lack the ability to quantify uncertainties in the decomposition results with respect to noisy data. In this work, we take the Bayesian approach to solve inverse problems as described in [15], that is, the inverse problem is formulated in a probabilistic sense in terms of random variables and their associated distributions. Regularization is now imposed via the prior probability distribution on the unknown, while model inaccuracies and measurement noise are accounted for in the likelihood function. The solution to a Bayesian inverse problem, called the posterior distribution, is the conditional distribution of the unknown given an observation of the data. Assuming that the components \mathbf{g} , \mathbf{h} and the noise ϵ are mutually independent, the posterior distribution associated with the inverse problem (1) is given by Bayes' theorem [15] as

$$\pi_{\text{post}}(\mathbf{g}, \mathbf{h} | \mathbf{y} = \mathbf{y}^*) \propto \pi_{\text{like}}(\mathbf{y} = \mathbf{y}^* | \mathbf{g}, \mathbf{h}) \pi_{\text{prior}}(\mathbf{g}) \pi_{\text{prior}}(\mathbf{h}). \quad (2)$$

Here $\mathbf{y}^* \in \mathbb{R}^m$ is the observed data, π_{like} is the likelihood function, π_{prior} is the prior distribution and π_{post} is the posterior distribution. Characterizing the posterior does not only give statistical estimates of the unknown, it also provides the related uncertainties in contrary to standard regularization techniques.

The formulation of prior distributions in Bayesian inverse problems is crucial for obtaining accurate estimates of the unknown and ensuring that its assumed properties

are properly enforced. In this work, we focus on two classes of priors: smoothness priors for representing the component \mathbf{h} , and priors that promote the piecewise constant structure for representing the component \mathbf{g} . One way of modeling smoothness priors is to construct prior distributions that impose smoothness regularity in a specific function space. These models include Gaussian priors that are realized in Sobolev spaces [16, 17] and Besov priors that are realized in Besov spaces [18, 19]. These models offer a consistent representation of smoothness and provide explicit control over it through the choice of prior parameters. The modeling of priors that promote piecewise constants is an active area of research, with several approaches available such as heavy-tailed priors [20–24], hierarchical shrinkage priors [25–29], machine-learning priors [30–32], and Haar-wavelet-based Besov priors [33–36]. Each of these methods has its strengths and limitations and should be selected based on the specific constraints of the problem at hand. We focus primarily on Besov priors as they offer a flexible framework for modeling both smooth and piecewise constant structures, while also allowing efficient computation and interpretable parameter choices.

The selection of parameters, which controls the relative contribution of each component’s prior information, is crucial for obtaining a balanced decomposition under the two-component model. In classical regularization methods, these parameters are often tuned manually based on visual quality, and there has been limited work on automatic parameter selection for decomposition, e.g., [8]. However, in the Bayesian framework, we can include these parameters as hyperparameters and estimate them jointly with the decomposition solution via the posterior. The main challenges lie in how to design priors and hyperpriors to ensure the components are well separated.

In this paper, we propose two Bayesian methods to solve linear inverse problems, where the unknown consists of two components with different properties. In the first method, we introduce a novel way of combining two distinct Besov priors by formulating a two-Besov decomposition model. We utilize the Besov prior with a Haar wavelet basis to impose jump discontinuities and the Besov prior with a smooth wavelet to impose smoothness. The No-U-Turn sampler (NUTS) [37] was applied to sample the posterior. In the second method, we propose a new hierarchical posterior to incorporate the parameters that control the strengths of the priors as hyperparameters. In this method, we use a combination of a hierarchical Gaussian prior on the discrete derivative to impose sparsely located jumps and a Besov prior with a smooth wavelet to impose localized smoothness. To sample this hierarchical posterior, we introduce a Gibbs sampling scheme, where marginal distributions either have closed-form expressions or can be effectively sampled using a Randomize-Then-Optimize (RTO) method [36, 38]. Both methods are tested on 1D and 2D deconvolution problems. The numerical results indicate that the decomposition method yields better reconstructions compared to methods using a single Besov prior. Furthermore, the hierarchical posterior can achieve automatic parameter selection for decomposition problems.

The main contributions of this paper are:

- We introduce Bayesian decomposition methods that can jointly recover smooth and

piecewise constant components and quantify uncertainties in the reconstruction.

- We propose a novel two-Besov decomposition model that incorporates two distinct Besov priors within a unified Bayesian framework.
- We propose a new hierarchical posterior to achieve automatic parameter selection in decomposition problems.
- We introduce a Gibbs sampling algorithm to sample the posteriors in the proposed methods while estimating the prior strength parameters simultaneously.
- We demonstrate the performance of our methods in 1D and 2D deconvolution problems.

This paper is structured as follows. In Section 2 we briefly review the concepts of wavelets and Besov priors and introduce a Bayesian decomposition model that combines two different Besov priors. In Section 3 we present a hierarchical posterior to include prior parameters as hyperparameters for a two-component linear Bayesian inverse problem. Additionally, we derive a Gibbs sampling method for posterior inference and parameter estimation. In Section 4 we illustrate our computational methods on deconvolution problems and showcase the properties of the models addressed. We end the paper with a conclusion in Section 5.

2. Besov decomposition

Besov priors are wavelet-based and allow explicit control over regularity in a class of smoothness spaces called Besov spaces. These priors are flexible, and depending on the prior setup, they can be used to impose either piecewise constant or different orders of smoothness.

2.1. Besov priors and wavelets

Before defining Besov priors, we briefly recall how to construct orthonormal wavelet basis on $L^2(\mathbb{R}^d)$ and $L^2(\mathbb{T}^d)$, where \mathbb{T}^d is the d -dimensional torus with $d \in \mathbb{N}$.

We first define the combined dilation and translation $f_{j,k}$ of a function $f \in L^2(\mathbb{R})$ as

$$f_{j,k}(x) = 2^{j/2} f(2^j x - k) \quad \text{for a.e. } x \in \mathbb{R}, \quad (3)$$

where j and k are integers. We denote the scaled and translated scaling and wavelet functions by $\psi_{j,k,0} = \phi_{j,k}$ and $\psi_{j,k,1} = \psi_{j,k}$. Whenever the collection $\{\psi_{0,k,0} \mid k \in \mathbb{Z}\} \cup \{\psi_{j,k,1} \mid j \in \mathbb{N}_0, k \in \mathbb{Z}\}$ forms an orthonormal basis of $L^2(\mathbb{R})$, the function ψ is said to be a wavelet, and ϕ is called a scaling function.

Following [39], we let $\phi, \psi \in C^r(\mathbb{R})$ with $r \geq 1$ be compactly supported scaling and wavelet functions, respectively. There exist choices of such wavelets ψ , where the associated scaling function ϕ generates a multiresolution analysis (MRA) of $L^2(\mathbb{R})$. An example is the Daubechies wavelet of order M , denoted by DB(M)-wavelet in the following, which is supported in $[0, 2M - 1]$ and belongs to $C^{\gamma M}(\mathbb{R})$ for $\gamma \approx 0.2075$ [40].

Next, we need to lift the one-variable wavelet and scaling functions to $L^2(\mathbb{R}^d)$. One way of generating an MRA on $L^2(\mathbb{R}^d)$ is to use a tensor-product of MRAs on $L^2(\mathbb{R})$. Define the index sets as $\mathcal{L}_0 = \{0, 1\}^d$ and $\mathcal{L}_1 = \mathcal{L}_0 \setminus \{0, 0, \dots, 0\}$. Then, for any $\ell \in \mathcal{L}_0$, we define the generators as

$$\psi_{j,k,\ell}(x) = \prod_{i=1}^d \psi_{j,k_i,\ell_i}(x_i), \quad \text{for a.e. } x = (x_1, x_2, \dots, x_d) \in \mathbb{R}^d, \quad (4)$$

where $j \in \mathbb{N}_0$, $k \in \mathbb{Z}^d$ and $\ell = (\ell_1, \ell_2, \dots, \ell_d) \in \mathcal{L}_0$. Note that $\ell = (0, 0, \dots, 0)$ corresponds to the scaling function, while each $\ell \in \mathcal{L}_1$ corresponds to the $2d - 1$ wavelet functions. The collection $\{\psi_{0,k,(0,0,\dots,0)}\}$, $k \in \mathbb{Z}^d\} \cup \{\psi_{j,k,\ell} \mid j \in \mathbb{N}_0, k \in \mathbb{Z}^d, \ell \in \mathcal{L}_1\}$ forms an orthonormal basis of $L^2(\mathbb{R}^d)$ [41].

The orthonormal wavelet basis of $L^2(\mathbb{R}^d)$ can be used to create an orthonormal basis of $L^2(\mathbb{T}^d)$ by periodization. Define the index set $\mathcal{K}_j = \{k \in \mathbb{Z}^d \mid 0 \leq k_1, k_2, \dots, k_d \leq 2^j - 1\}$. Then the 1-periodization of the wavelets in (4) is defined, for $j \in \mathbb{N}_0, k \in \mathcal{K}_j, \ell \in \mathcal{L}_0$, as

$$\psi_{j,k,\ell}^{\text{per}}(x) = \sum_{n \in \mathbb{Z}^d} \psi_{j,k,\ell}(x - n), \quad \text{for a.e. } x \in \mathbb{T}^d. \quad (5)$$

Set the index set as $\mathcal{I}_\psi = \{(0, 0, 0, \dots, 0)\} \cup \{j \in \mathbb{N}_0, k \in \mathcal{K}_j, \ell \in \mathcal{L}_1\}$ then the collection $\{\psi_{j,k,\ell}^{\text{per}}, (j, k, \ell) \in \mathcal{I}_\psi\}$ is an orthonormal basis of $L^2(\mathbb{T}^d)$ [42]. The 1-periodic orthonormal wavelet basis can, under conditions on its smoothness, be used to define a class of smoothness spaces known as Besov spaces [43].

Definition 1. Let $s > 0, p \in [1, \infty)$, and assume that the wavelets belong to $C^r(\mathbb{T}^d)$ with $r > s$. We define the Besov spaces on \mathbb{T}^d as the family of spaces

$$B_{p,p}^s(\mathbb{T}^d) := \left\{ f \in L^p(\mathbb{T}^d) : \|f\|_{B_{p,p}^s(\mathbb{T}^d)} < \infty \right\}, \quad (6)$$

with Besov norms defined by

$$\|f\|_{B_{p,p}^s(\mathbb{T}^d)} = \left(\sum_{(j,k,\ell) \in \mathcal{I}_\psi} 2^{jp(s + \frac{d}{2} - \frac{d}{p})} |w_{j,k,\ell}|^p \right)^{1/p}. \quad (7)$$

where $w_{j,k,\ell}$ are the wavelet coefficients given by

$$w_{j,k,\ell} = \int_{\mathbb{T}^d} f(x) \overline{\psi_{j,k,\ell}^{\text{per}}(x)} dx. \quad (8)$$

Besov priors can now be constructed as a wavelet expansion where the expansion coefficients are chosen at random according to generalized Gaussian random variables. For $p \in [1, \infty)$ we define a sequence $\Xi = \{\xi_{j,k,\ell}, (j, k, \ell) \in \mathcal{I}_\psi\}$ of independent identically distributed (i.i.d.) generalized Gaussian random variables, where each $\xi_{j,k,\ell}$ is distributed according to a Lebesgue density given by

$$\pi_\xi(x) = \frac{1}{c_p} \exp(-|x|^p), \quad c_p = \int_{\mathbb{R}} \exp(-|x|^p) dx, \quad x \in \mathbb{R}. \quad (9)$$

To define the random wavelet expansion, we first have to establish the probability space for the coefficient sequence. Let \mathbb{Q}_p be the measure associated with a one-dimensional generalized Gaussian random variable on $(\mathbb{R}, \mathcal{B}(\mathbb{R}))$. Formally, we take the countable product of these one-dimensional spaces:

$$\Omega = \mathbb{R}^\infty, \quad \mathcal{B} = \bigotimes_{n \in \mathbb{N}} \mathcal{B}(\mathbb{R}), \quad \mathbb{Q} = \bigotimes_{n \in \mathbb{N}} \mathbb{Q}_p. \quad (10)$$

By Kolmogorov's extension theorem, the infinite product measure \mathbb{Q} is well-defined on the cylinder σ -algebra \mathcal{B} , giving $(\Omega, \mathcal{B}, \mathbb{Q})$ a complete probability-space structure for the sequence Ξ .

Definition 2. Let $s > 0, p \in [1, \infty)$ and Ξ be the sequence of i.i.d. generalized Gaussian random variables. We define a random wavelet expansion as the mapping

$$T : \Omega \rightarrow B_{p,p}^s(\mathbb{T}^d), \quad \Xi \mapsto \sum_{(j,k,\ell) \in \mathcal{I}_\psi} 2^{-j(s+\frac{d}{2}-\frac{d}{p})} \xi_{j,k,\ell}(\omega) \psi_{j,k,\ell}^{\text{per}}, \quad \omega \in \Omega. \quad (11)$$

We say that the random wavelet expansion generates a Besov random variable $T_{p,\psi}^s$.

The random wavelet expansion in (11) almost surely takes values in the space $B_{p,p}^t(\mathbb{T}^d)$ if and only if $t < s - \frac{d}{p}$ [18] and generates a Besov probability measure defined by a pushforward measure $\mathbb{Q} \circ T^{-1}$ [19]. Formally, this gives rise to a Besov prior with Lebesgue density given by

$$\pi_{T_{p,\psi}^s}(f) \propto \exp(-\|f\|_{B_{p,p}^s(\mathbb{T}^d)}^p). \quad (12)$$

However, the Lebesgue density in (12) is not well-defined as a function on $B_{p,p}^s(\mathbb{T}^d)$ since the space is infinite-dimensional. Instead, we interpret the prior as a Radon measure $\mathbb{Q} \circ T^{-1}$ that coincides with the finite-dimensional exponential-power densities on all wavelet cylinder sets.

2.2. Discrete Besov priors

Besov priors can be discretized by truncating the wavelet expansion in (11) to the finite index set $\mathcal{I}_{\psi,J} := \{(0, 0, \dots, 0)\} \cup \{j \in \{0, 1, \dots, J-1\}, k \in \mathcal{K}_j, \ell \in \mathcal{L}_1\}$ for some integer $J \geq 1$, which results in a $|\mathcal{I}_{\psi,J}| = 2^{Jd}$ coefficient representation of f . Set $n = 2^{Jd}$ and let $\mathbf{S} \in \mathbb{R}^{n \times n}$ be the Besov scaling matrix which is a diagonal matrix with entries

$$\mathbf{S}_{0,0} = 1, \quad \mathbf{S}_{i,i} = 2^{j(s+d/2-d/p)}, \quad \text{for } 2^{jd} + 1 \leq i \leq 2^{(j+1)d}. \quad (13)$$

Let $\mathbf{W}_\psi \in \mathbb{R}^{n \times n}$ be a discrete wavelet transform associated to the wavelet ψ in such a way that

$$\mathbf{W}_\psi \mathbf{f} \approx \left\{ \langle f, \psi_{j,k,\ell}^{\text{per}} \rangle_{L^2(\mathbb{T}^d)} \right\}_{(j,k,\ell) \in \mathcal{I}_{\psi,J}}. \quad (14)$$

We will use the fast wavelet transform [44] implemented in the Pywavelets module [45] for computing the wavelet transform with \mathbf{W}_ψ . The continuous Besov norm can be approximated by a discrete version as

$$\|f\|_{B_{p,p}^s(\mathbb{T}^d)} \approx \|\mathbf{S}\mathbf{W}_\psi \mathbf{f}\|_p. \quad (15)$$

The discrete Besov prior distribution is then given by

$$\pi_{T_{p,\psi}^s}(\mathbf{f}) \propto \exp\left(-\lambda\|\mathbf{S}\mathbf{W}_\psi\mathbf{f}\|_p^p\right), \quad (16)$$

where $\lambda > 0$ is the prior strength parameter.

2.3. The posterior for Bayesian decomposition

We consider a decomposition model in which the unknown f is split into two components, $f = \mathbf{g} + \mathbf{h}$, with different structural properties. To impose piecewise constant characteristics, we let \mathbf{g} follow a Besov prior $\mathbf{g} \sim T_{p_g, \psi_g}^{s_g}$ where ψ_g is the Haar wavelet. To impose smoothness in \mathbf{h} , we assign a Besov prior $\mathbf{h} \sim T_{p_h, \psi_h}^{s_h}$, with ψ_h a smooth wavelet, e.g., a high-order Daubechies wavelet.

Assuming that \mathbf{g} and \mathbf{h} are independent, the prior distribution factorizes as a product measure of the form

$$\pi_{\text{prior}}(\mathbf{g})\pi_{\text{prior}}(\mathbf{h}) \propto \exp\left(-\lambda_g\|\mathbf{S}_g\mathbf{W}_{\psi_g}\mathbf{g}\|_{p_g}^{p_g} - \lambda_h\|\mathbf{S}_h\mathbf{W}_{\psi_h}\mathbf{h}\|_{p_h}^{p_h}\right), \quad (17)$$

where $\lambda_g, \lambda_h > 0$ are the prior strength parameters associated to the components. This formulation allows us to combine different Besov priors in one posterior.

In the inverse problem defined in (1), we assume the noise is Gaussian $\epsilon \sim N(\mathbf{0}, \sigma^2\mathbf{I}_m)$ with zero mean and covariance matrix $\sigma^2\mathbf{I}_m$, where $\sigma > 0$ and $\mathbf{I}_m \in \mathbb{R}^{m \times m}$ is the identity matrix. This assumption leads to a likelihood function for the components given by

$$\pi_{\text{like}}(\mathbf{y} = \mathbf{y}^* | \mathbf{g}, \mathbf{h}) \propto \exp\left(-\frac{1}{2\sigma^2}\|\mathbf{A}(\mathbf{g} + \mathbf{h}) - \mathbf{y}^*\|_2^2\right). \quad (18)$$

The solution to the Bayesian decomposition problem is given by the posterior distribution, which combines the prior and likelihood. According to Bayes' theorem [15], the posterior is proportional to the product of the likelihood and the prior, i.e.,

$$\begin{aligned} \pi_{\text{post}}(\mathbf{g}, \mathbf{h} | \mathbf{y} = \mathbf{y}^*) \propto \exp\left(-\frac{1}{2\sigma^2}\|\mathbf{A}(\mathbf{g} + \mathbf{h}) - \mathbf{y}^*\|_2^2 \right. \\ \left. - \lambda_g\|\mathbf{S}_g\mathbf{W}_{\psi_g}\mathbf{g}\|_{p_g}^{p_g} - \lambda_h\|\mathbf{S}_h\mathbf{W}_{\psi_h}\mathbf{h}\|_{p_h}^{p_h}\right). \end{aligned} \quad (19)$$

When the prior strength parameters λ_g and λ_h are fixed, we use the No-U-Turn sampler (NUTS) [37] to sample from the posterior distribution in (19). NUTS is a Hamiltonian Markov chain Monte Carlo method with automatic adaptive step size control, which usually makes it efficient and eliminates the need for manual tuning of the sampler. The negative log posterior of (19) is almost everywhere differentiable for all choices of prior parameters $s_g, s_h > 0$ and $p_g, p_h \in [1, \infty)$, which makes NUTS applicable in this setting.

In decomposition problems, the results strongly depend on the strength parameters λ_g and λ_h , which define the balance between two components. The choice of the strength parameters is crucial and challenging. Under Bayesian statistics, we can introduce

a hierarchical model to incorporate both parameters as unknown random variables, called hyperparameters, in the posterior[‡]. Unfortunately, even when the two priors are constructed from structurally different wavelets, the resulting hierarchical model suffers from an identifiability problem. In general, two wavelet bases have high mutual coherence defined as the maximum absolute value of the inner product between two wavelet functions from different bases [46]. In particular, we see a large coherence between scaling functions and other low-frequency wavelets from the different bases. This high mutual coherence leads to a lack of identifiability in the posterior distribution. When the strength parameters are considered as random variables, it becomes difficult to distinguish the contributions between two Besov priors, as they can represent similar features in the unknown. This lack of identifiability can result in a multimodal posterior, as different parameter choices may cause different priors to dominate the reconstruction. Sampling from multimodal posteriors is a well-known challenge for Gibbs sampling and Markov chain Monte Carlo methods in general, and addressing it is beyond the scope of this paper. The identifiability issues are numerically illustrated in Section 4.

To overcome this issue, we abandon the Besov prior for the piecewise constant component and instead place a hierarchical Gaussian prior on the discrete gradient. This change enforces sparsity in the physical domain rather than in the wavelet domain and helps mitigate coherence issues between the representation systems underlying the two priors.

3. Hierarchical Gaussian-Besov decomposition method

In this section, we propose an alternative prior for the piecewise constant component \mathbf{g} by modeling its discrete gradient as a Gaussian random vector with a diagonal covariance matrix. The associated variance parameters are treated as hyperparameters. Combined with a smooth Besov prior for \mathbf{h} , this yields a new hierarchical Bayesian decomposition model that can be sampled efficiently with Gibbs updates and that avoids the identifiability issues of the two-Besov formulation.

Assume that the gradient of \mathbf{g} , denoted $\mathbf{D}_d \mathbf{g} \in \mathbb{R}^{dn}$, follows a Gaussian distribution $\mathcal{N}(\mathbf{0}, \mathbf{\Lambda})$ with mean $\mathbf{0}$ and covariance $\mathbf{\Lambda}$. The 1D gradient operator is defined using a forward finite difference scheme with periodic boundary conditions as

$$\mathbf{D}_1 = \begin{bmatrix} -1 & 1 & & & \\ & -1 & 1 & & \\ & & \ddots & \ddots & \\ & & & -1 & 1 \\ 1 & & & & -1 \end{bmatrix} \in \mathbb{R}^{n \times n}. \quad (20)$$

The matrix representation of the higher-dimensional gradient operator can be generated

[‡] The model is derived in Appendix A. For numerical experiments, see Figures 6 and 7.

by \mathbf{D}_1 and the Kronecker product, e.g., the 2D gradient operator is given as

$$\mathbf{D}_2 = \begin{bmatrix} \mathbf{I}_n \otimes \mathbf{D}_1 \\ \mathbf{D}_1 \otimes \mathbf{I}_n \end{bmatrix} \in \mathbb{R}^{2n \times n}, \quad (21)$$

where \otimes denotes the Kronecker product. Referring to the work in [27], we consider a diagonal covariance $\mathbf{\Lambda}$ and assume that the diagonal entries are i.i.d. random variables following the inverse gamma distribution $\mathcal{IG}(\alpha_1, \beta_1)$. This hierarchical Gaussian prior imposes sparsity on the gradient of \mathbf{g} . For the smooth component \mathbf{h} , we continue to use a discrete Besov prior $\mathbf{h} \sim T_{p_h, \psi_h}^{s_h}$ with $p_h = 2$ and a smooth wavelet ψ_h . Furthermore, we set the prior strength parameter λ_h as a hyperparameter following the gamma distribution $\mathcal{G}(\alpha_2, \beta_2)$, which is conjugate to the Gaussian distribution. Combining with the Gaussian likelihood, we form the joint posterior of the components and hyperparameters as

$$\begin{aligned} \pi_{\text{post}}(\mathbf{g}, \mathbf{h}, \mathbf{\Lambda}, \lambda_h | \mathbf{y} = \mathbf{y}^*) &\propto \pi_{\text{like}}(\mathbf{y} = \mathbf{y}^* | \mathbf{g}, \mathbf{h}) \pi_{\text{prior}}(\mathbf{g} | \mathbf{\Lambda}) \pi_{\text{prior}}(\mathbf{h} | \lambda_h) \pi_{\text{hyp}}(\mathbf{\Lambda}) \pi_{\text{hyp}}(\lambda_h) \\ &\propto \lambda_h^{n/2 + \alpha_2 - 1} \left(\prod_{i=1}^{dn} \Lambda_{i,i} \right)^{-\alpha_1 - 3/2} \\ &\quad \exp\left(-\frac{1}{2\sigma^2} \|\mathbf{A}(\mathbf{g} + \mathbf{h}) - \mathbf{y}^*\|_2^2 - \frac{1}{2} \|\mathbf{\Lambda}^{-1/2} \mathbf{D}_d \mathbf{g}\|_2^2\right. \\ &\quad \left. - \frac{\lambda_h}{2} \|\mathbf{S}_h \mathbf{W}_{\psi_h} \mathbf{h}\|_2^2 - \beta_2 \lambda_h - \beta_1 \sum_{i=1}^{dn} \Lambda_{i,i}^{-1}\right). \end{aligned} \quad (22)$$

To sample from the posterior in (22) we use a Gibbs sampling scheme outlined in Algorithm 1, which samples components and hyperparameters sequentially from their marginal distributions given as follows.

$$\begin{aligned} \pi_1(\mathbf{g} | \mathbf{y}^*, \mathbf{h}, \mathbf{\Lambda}) &\propto \exp\left(-\frac{1}{2\sigma^2} \|\mathbf{A}(\mathbf{g} + \mathbf{h}) - \mathbf{y}^*\|_2^2 - \frac{1}{2} \|\mathbf{\Lambda}^{-1/2} \mathbf{D}_d \mathbf{g}\|_2^2\right), \\ \pi_2(\mathbf{h} | \mathbf{y}^*, \mathbf{g}, \lambda_h) &\propto \exp\left(-\frac{1}{2\sigma^2} \|\mathbf{A}(\mathbf{g} + \mathbf{h}) - \mathbf{y}^*\|_2^2 - \frac{\lambda_h}{2} \|\mathbf{S}_h \mathbf{W}_{\psi_h} \mathbf{h}\|_2^2\right), \\ \pi_3(\mathbf{\Lambda} | \mathbf{g}) &\propto \left(\prod_{i=1}^{dn} \Lambda_{i,i} \right)^{-\alpha_1 - 3/2} \exp\left(-\frac{1}{2} \|\mathbf{\Lambda}^{-1/2} \mathbf{D}_d \mathbf{g}\|_2^2 - \beta_1 \sum_{i=1}^{dn} \Lambda_{i,i}^{-1}\right), \\ \pi_4(\lambda_h | \mathbf{h}) &\propto (\lambda_h)^{n/2 + \alpha_2 - 1} \exp\left(-\frac{\lambda_h}{2} \|\mathbf{S}_h \mathbf{W}_{\psi_h} \mathbf{h}\|_2^2 - \beta_2 \lambda_h\right). \end{aligned}$$

To sample the marginal distributions π_1 and π_2 , we notice that they are Gaussian and can be sampled efficiently using the Randomize-Then-Optimize (RTO) method [36,38]. RTO draws samples from a Gaussian distribution by solving the following random perturbed

linear least squares problems

$$\arg \min_{\mathbf{g}} \frac{1}{2} \left\| \begin{bmatrix} \frac{1}{\sigma} \mathbf{A} \\ \mathbf{\Lambda}^{-1/2} \mathbf{D}_d \end{bmatrix} \mathbf{g} - \begin{bmatrix} \frac{1}{\sigma} \mathbf{y}^* - \frac{1}{\sigma} \mathbf{A} \mathbf{h} \\ \mathbf{0} \end{bmatrix} - \boldsymbol{\eta}^* \right\|_2^2, \quad \boldsymbol{\eta} \sim \mathcal{N}(\mathbf{0}, \mathbf{I}_{m+dn}), \quad (24a)$$

$$\arg \min_{\mathbf{h}} \frac{1}{2} \left\| \begin{bmatrix} \frac{1}{\sigma} \mathbf{A} \\ \sqrt{\lambda_h} \mathbf{S}_h \mathbf{W}_{\psi_h} \end{bmatrix} \mathbf{h} - \begin{bmatrix} \frac{1}{\sigma} \mathbf{y}^* - \frac{1}{\sigma} \mathbf{A} \mathbf{g} \\ \mathbf{0} \end{bmatrix} - \boldsymbol{\zeta}^* \right\|_2^2, \quad \boldsymbol{\zeta} \sim N(\mathbf{0}, \mathbf{I}_{m+n}), \quad (24b)$$

where $\boldsymbol{\eta}^*$ and $\boldsymbol{\zeta}^*$ are realizations of $\boldsymbol{\eta}$ and $\boldsymbol{\zeta}$, respectively. We solve the linear least squares problems using a CGLS algorithm [47]. To sample the covariance matrix $\mathbf{\Lambda}$ we notice that π_3 is an independent product of

$$\mathbf{\Lambda}_{i,i} \sim \mathcal{IG}(\alpha_1 + 1/2, \beta_1 + (\mathbf{D}_d \mathbf{g})_i^2), \quad (25)$$

such that we can sample each element independently and directly from an inverse gamma distribution. At last, π_4 is a gamma distribution

$$\lambda_h \sim \mathcal{G}\left(n/2 + \alpha_2, \beta_2 + \frac{1}{2} \|\mathbf{S}_h \mathbf{W}_{\psi_h} \mathbf{h}\|_2^2\right), \quad (26)$$

which can also be sampled directly with given α_2 and β_2 .

Algorithm 1 Gibbs sampling procedure

Require: The number of samples n_{samp} , initial guesses $\mathbf{g}^0, \mathbf{h}^0, \mathbf{\Lambda}^0, \lambda_h^0$, and data \mathbf{y}^* .

- 1: **for** $i = 1, \dots, n_{\text{samp}}$ **do**
 - 2: //Sampling components
 - 3: $\mathbf{g}^i \sim \pi_1(\cdot | \mathbf{y}^*, \mathbf{h}^{i-1}, \mathbf{\Lambda}^{i-1})$: Sample by solving (24a) using CGLS.
 - 4: $\mathbf{h}^i \sim \pi_2(\cdot | \mathbf{y}^*, \mathbf{g}^i, \lambda_h^{i-1})$: Sample by solving (24b) using CGLS.
 - 5: // Sampling hyperparameters
 - 6: $\mathbf{\Lambda}^i \sim \pi_3(\cdot | \mathbf{g}^i)$: Sample directly from an inverse gamma distribution defined in (25).
 - 7: $\lambda_h^i \sim \pi_4(\cdot | \mathbf{h}^i)$: Sample directly from a gamma distribution defined in (26).
 - 8: **end for**
 - 9: **return** $\{\mathbf{g}^i, \mathbf{h}^i, \mathbf{\Lambda}^i, \lambda_h^i\}_{i=1}^{n_{\text{samp}}}$
-

Remark 1. To reduce the correlation between \mathbf{g} and \mathbf{h} , we enforce a zero-mean condition on \mathbf{g} , i.e., $\mathbb{E}[\mathbf{g}] = 0$, so that the mean of \mathbf{h} agrees with the mean of the combined signal $\mathbf{f} = \mathbf{g} + \mathbf{h}$. To achieve this, we define the new components as $\tilde{\mathbf{g}}$ and $\tilde{\mathbf{h}}$, and their samples are computed as

$$\begin{aligned} \tilde{\mathbf{g}}^i &= \mathbf{g}^i - \mathbb{E}[\mathbf{g}^i], \\ \tilde{\mathbf{h}}^i &= \mathbf{h}^i + \mathbb{E}[\mathbf{g}^i], \end{aligned}$$

where \mathbf{g}^i and \mathbf{h}^i are obtained from Algorithm 1.

4. Numerical experiments

In this section, we numerically evaluate the performance of the two proposed methods for reconstructing a signal composed of a piecewise constant component and a smooth component. We focus on linear deconvolution problems. The first two tests are one-dimensional problems, which allow for an in-depth investigation of the proposed methods. The third test is used to demonstrate the performance of the proposed hierarchical method on a two-dimensional problem.

4.1. One dimensional deconvolution: Two-Besov prior method

We consider a one-dimensional periodic deconvolution problem, that is, we want to identify an unknown $f : \mathbb{T} \rightarrow \mathbb{R}$ from noisy convolved data. The periodic deconvolution problem can be modeled as an inverse problem

$$y(t) = \int_{\mathbb{T}} A(t-x)f(x) dx, \quad (27)$$

where y is the observed data and $A \in \mathcal{C}^\infty(\mathbb{T})$ is a smooth convolution kernel. In this test, we use a 1-periodic, centered Gaussian kernel with standard deviation $\sigma_{\text{ker}} > 0$, i.e.,

$$A(x) = \frac{1}{\sqrt{2\pi}\sigma_{\text{ker}}} \sum_{k=-\infty}^{\infty} \exp\left(\frac{-(x+k)^2}{2\sigma_{\text{ker}}^2}\right), \quad x \in \mathbb{T}. \quad (28)$$

The ground truth signal $\mathbf{f}_{\text{truth}}$ is constructed as a linear combination of Haar wavelets and DB(8) wavelets, discretized on a uniform grid of 512 points over the interval $[0, 1)$ with a truncation parameter set to $J = 9$. The convolution operator A is discretized on the same grid, resulting in a discrete forward operator $\mathbf{A} \in \mathbb{R}^{512 \times 512}$. This operator is implemented as a circulant matrix corresponding to the Gaussian convolution kernel in (28) truncated at $\pm 3\sigma_{\text{ker}}$ with $\sigma_{\text{ker}} = 0.01$. The degraded data \mathbf{y}^* is generated by adding 10% Gaussian noise ϵ , i.e., $\frac{\|\epsilon\|_2}{\|\mathbf{A}\mathbf{f}_{\text{true}}\|_2} = 0.1$, on $\mathbf{A}\mathbf{f}_{\text{true}}$. Figure 1 displays the ground truth signal \mathbf{f}_{true} , its components \mathbf{g} and \mathbf{h} , and the noisy observation \mathbf{y}^* .

In this test scenario, we study the performance of the method with two Besov priors introduced in Section 2. We use the Haar wavelet ψ_g for \mathbf{g} and the DB(8) wavelet ψ_h for \mathbf{h} . The prior parameters are set as $s_g = s_h = p_g = p_h = 1$. We first fix $\lambda_g = \lambda_h = 1$ to analyze the uncertainty quantification properties of the method and compare it to the method using a single Besov prior in terms of both sampling efficiency and reconstruction quality. We then study the influence of varying λ_g and λ_h on the reconstruction quality.

For all experiments in this test, inference is performed using NUTS to generate 15 000 total samples, of which the first 5000 are discarded as burn-in. The remaining 10 000 samples are used to compute the posterior mean estimate, the 95% credible interval (CI), and the CI width. To assess sampling quality, we compute the effective sample size (ESS) over the entire grid and report the minimum, median, and maximum values. Additionally, we evaluate the autocorrelation function (ACF) at a representative

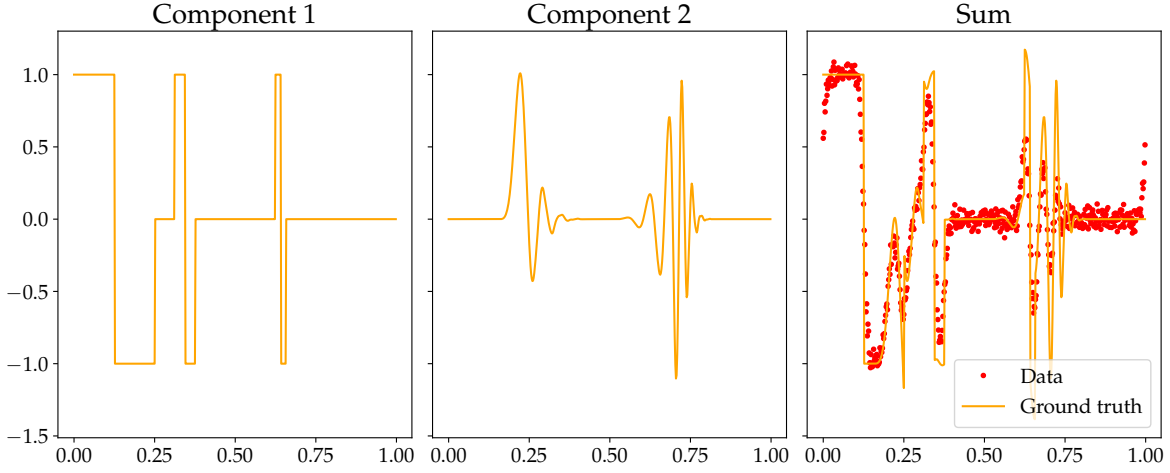


Figure 1: The ground truth signal and the degraded data (in red, to the right), together with the true piecewise constant component (to the left) and the smooth component (in the middle).

grid point to examine sample correlation. Reconstruction quality is measured using the relative error between the posterior mean and the ground truth \mathbf{f}_{true} .

Figure 2 shows the reconstruction and uncertainty quantification results from the method with two Besov priors. The posterior mean estimates for \mathbf{g} and \mathbf{h} carry the most features from the true components, and the mean of \mathbf{f} , whose samples are obtained by calculating the sum of corresponding \mathbf{g} and \mathbf{h} samples, successfully represents both the sharp transitions and smooth variations present in the ground truth. The plots of the CI widths in Figure 2 show that uncertainty is higher in the regions where both components contribute significantly, indicating that the decomposition introduces additional variability in these areas.

Next, we compare the performance of the two-Besov prior model (Haar+DB(8)) with that of standard single Besov priors (either Haar or DB(8) alone) applied directly to \mathbf{f} , using identical prior parameters and sampling settings as described above. As shown in Figure 3, it is obvious that the Haar Besov prior introduces staircasing artifacts, while the DB(8) Besov prior tends to oversmooth the reconstruction. In contrast, the proposed two-Besov model achieves a more balanced reconstruction, mitigating both types of artifacts and yielding a lower relative reconstruction error, as summarized in Table 1. Comparing the CI widths in Figure 3, we can see that the results from the single Besov prior exhibit generally lower uncertainty compared to the two-Besov method, likely due to the inherent nonuniqueness and the mutual coherence between the two representation systems used in the decomposition. Moreover, the decomposition samples show higher correlation, as evidenced by slower ACF decay and lower ESS values. This indicates that sampling the posterior for decomposition problems is more challenging. Nevertheless, the correlation remains within acceptable limits, and the samples are deemed sufficient for a reliable posterior estimation.

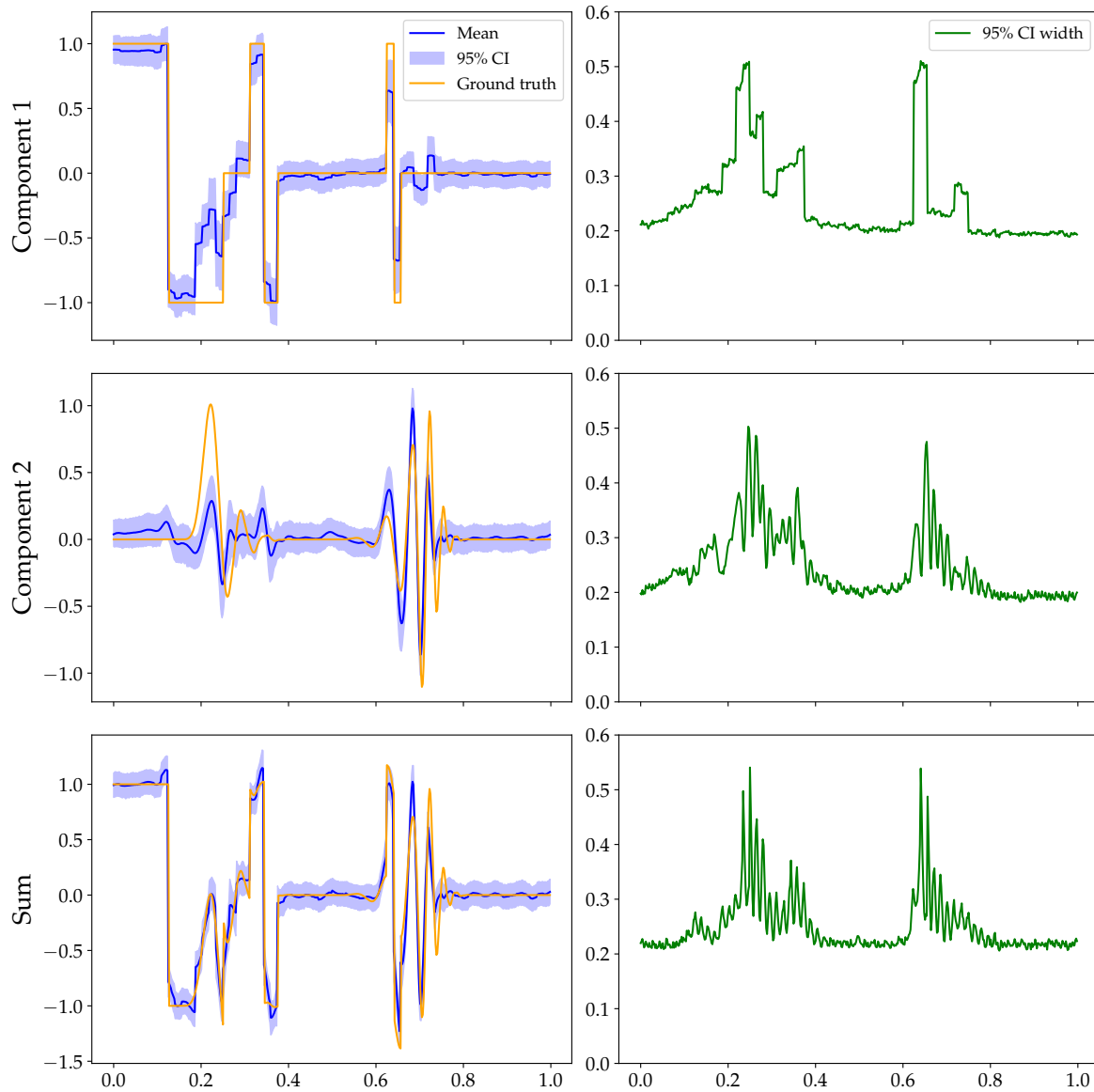


Figure 2: Posterior estimates using the Haar and DB(8) wavelets in the two-Besov prior decomposition model with the parameters $s_g = s_h = p_g = p_h = \lambda_g = \lambda_h = 1$.

Table 1: The effective sample sizes (ESS) and the relative errors.

| Method | ESS | | | Relative error |
|------------|---------|---------|---------|----------------|
| | Minimum | Median | Maximum | |
| Haar | 1318.68 | 6906.55 | 9047.97 | 0.378 |
| DB(8) | 1296.79 | 5947.35 | 9135.38 | 0.363 |
| Haar+DB(8) | 111.45 | 4500.12 | 6077.02 | 0.308 |

In the two-Besov decomposition model, the parameters λ_g and λ_h control the relative contributions of the components in the posterior. Their choices have a

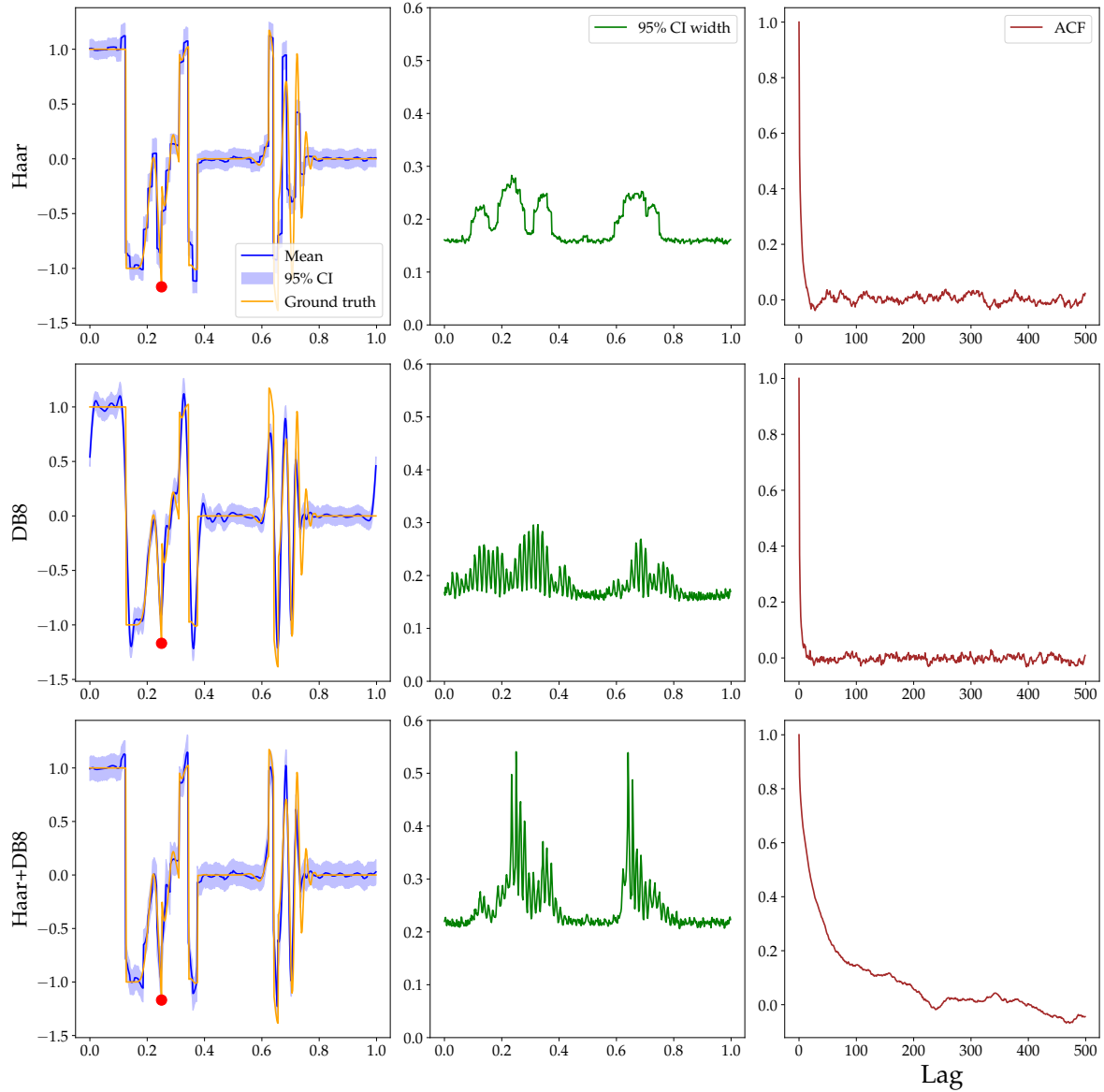


Figure 3: Posterior estimates and autocorrelation functions (ACFs) computed from the chains at a representative grid point (marked with a red dot). Row 1: One-Besov prior using Haar, i.e., DB(1), wavelets. Row 2: One-Besov prior using DB(8) wavelets. Row 3: Two-Besov prior model combining Haar and DB(8) wavelets (as in Section 2.3). All reconstructions use the same prior parameters $s = p = \lambda = 1$ for single Besov priors and $s_g = s_h = p_g = p_h = \lambda_g = \lambda_h = 1$ for the two-Besov model.

substantial impact on the results as illustrated in Figure 4. As λ_h increases, the second component progressively dominates the reconstruction, eventually becoming the primary contributor. Conversely, when $\lambda_g > \lambda_h$, the first component dominates. These results highlight the importance of selecting appropriate values for λ_g and λ_h to achieve a balanced and interpretable decomposition. This observation also motivates the second proposed method based on a hierarchical posterior.

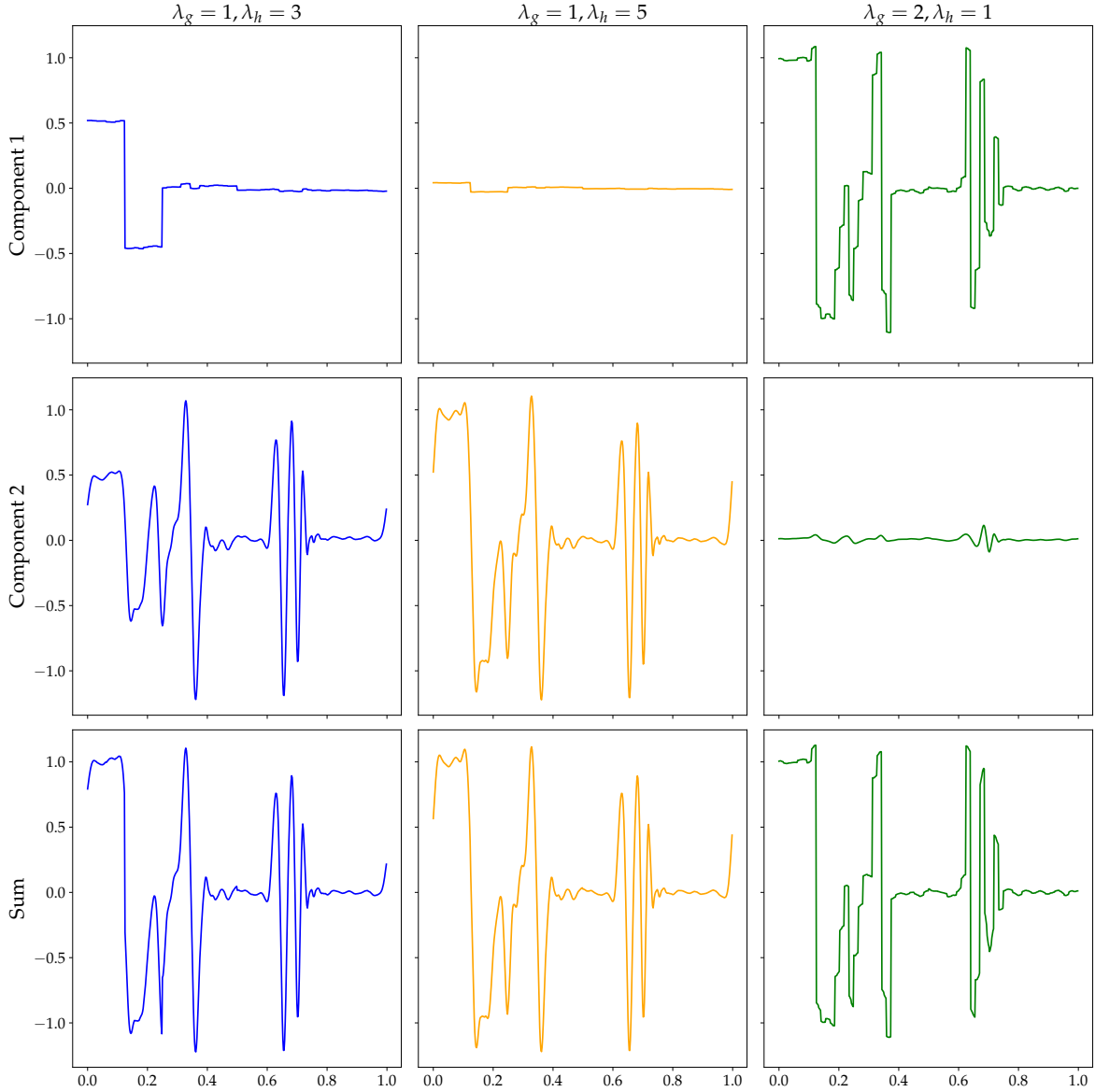


Figure 4: Posterior estimates for the decomposition method with different choices of prior strength parameters.

4.2. One dimensional deconvolution: Hierarchical decomposition method

In this test scenario, the ground truth signal \mathbf{f}_{true} is composed of a piecewise constant component and a smooth Gaussian component, both defined on the domain $[0, 1)$ and discretized at 128 equidistant points. The observed data is generated by convolving the signal with a periodic Gaussian kernel of standard deviation $\sigma_{\text{ker}} = 0.02$, followed by the addition of 5% Gaussian noise. This setup mirrors the setup described in Section 4.2. A visualization of the ground truth and the observed data is shown in Figure 5.

First, we test the hierarchical decomposition method with two Besov priors on this problem. The hierarchical posterior and the sampling scheme are given in Appendix A.

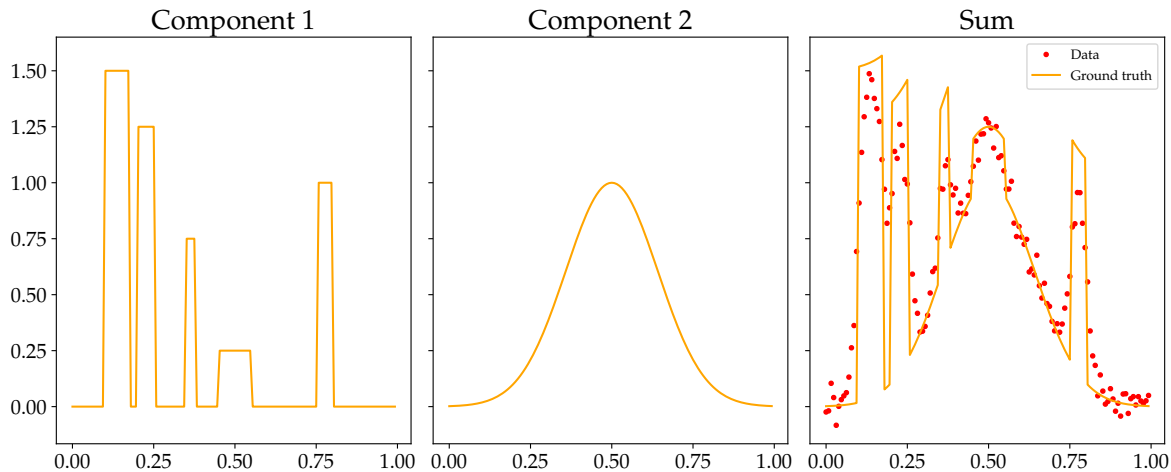


Figure 5: Ground truth (to the right) as a sum of the piecewise constant component (to the left) and the smooth component (in the middle) together with the degraded data (to the right).

We use the Haar wavelet for ψ_g and the DB(8) wavelet for ψ_h , with prior smoothness parameters set to $s_g = 1$ and $s_h = 3$, respectively. In the Gibbs sampler, we set $a_1 = a_2 = 2$ and $b_1 = b_2 = 10^{-3}$. We draw 1 000 000 samples and use the first 10 000 samples as burn-in, and thin the remaining samples by a factor of 200, resulting in 4950 samples for posterior analysis.

In Figure 6 we show the diagnostics of λ_g and λ_h including individual chains, histograms, cumulative means and ACFs. We can see that both chains exhibit good mixing, cumulative means converge quickly, and ACFs reduce to zero rapidly. However, λ_g is significantly smaller than λ_h , resulting in an imbalanced decomposition. This imbalance is evident in the posterior mean, where the component \mathbf{g} dominates, as shown in Figure 7. This test illustrates that a simple designed hierarchical decomposition method with two Besov priors fails due to identifiability limitations discussed in the end of Section 2.

Next, we test the method proposed in Section 3, where we combine a hierarchical Gaussian prior with a Besov prior. For the Besov prior, we use DB(8) wavelet for ψ_h and set $s_h = 3$. For the hyperparameters, we set $\alpha_1 = 1, \alpha_2 = 2$ and $\beta_1 = 10^{-5}, \beta_2 = 10^{-2}$. The number of samples, burn-in and thinning are the same as in the previous test.

In Figure 8 we show the posterior statistics of λ_h . Comparing with the posterior statistics of hyperparameters in two Besov priors case which is shown in Figure 6, we can see that the chain exhibits some correlation with occasional outliers, and the cumulative mean converges slower. The posterior estimates of both components and their sum \mathbf{f} are shown in Figure 9. We observe that the component \mathbf{g} captures nearly all ten jumps, estimating both their locations and magnitudes with reasonable accuracy. Furthermore, the posterior mean of \mathbf{f} provides a qualitatively accurate reconstruction of the unknown. According to the 95% CI width of \mathbf{f} , we see that higher uncertainties are observed near

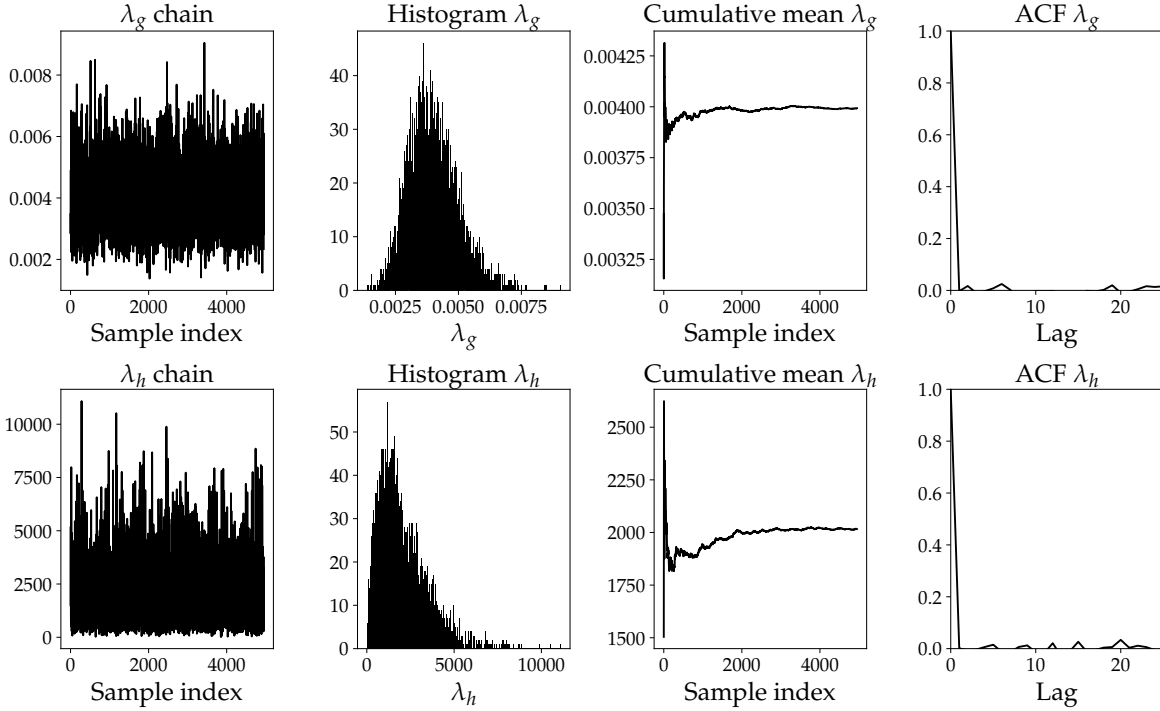


Figure 6: Posteriors of the hyperparameters λ_g and λ_h in the hierarchical decomposition method with two Besov priors.

Table 2: Comparison of two hierarchical decomposition methods.

| Two Besov priors | | | Hierarchical Gaussian with Besov | | |
|------------------|-----------------|---------|----------------------------------|-----------------|-----------|
| ESS λ_g | ESS λ_h | Rel_err | Min ESS $\mathbf{\Lambda}$ | ESS λ_h | Rel_error |
| 4893.45 | 4883.70 | 0.307 | 22.80 | 335.61 | 0.103 |

the jumps, reflecting that it's difficult to reconstruct high frequency information. In the last row of Figure 9, we also show the posterior statistics for $\mathbf{\Lambda}$, the covariance of the hierarchical Gaussian prior. It is obvious that $\mathbf{\Lambda}$ is sparse, and the locations of non-zero elements correspond to the jumps in the gradient. The uncertainty is large at those particular locations and essentially zero in the rest of the domain.

Finally, we quantitatively compare two hierarchical decomposition methods introduced in Appendix A with two Besov priors and in Section 3 with a hierarchical Gaussian and Besov prior. The results are summarized in Table 2. While the method with two Besov priors provides superior sampling efficiency, as measured by ESS of the hyperparameters, it fails to produce a balanced decomposition. In contrast, the method with a hierarchical Gaussian and a Besov prior is less efficient on sampling, but it successfully identifies hyperparameters that yield a decomposition with substantially lower relative error.

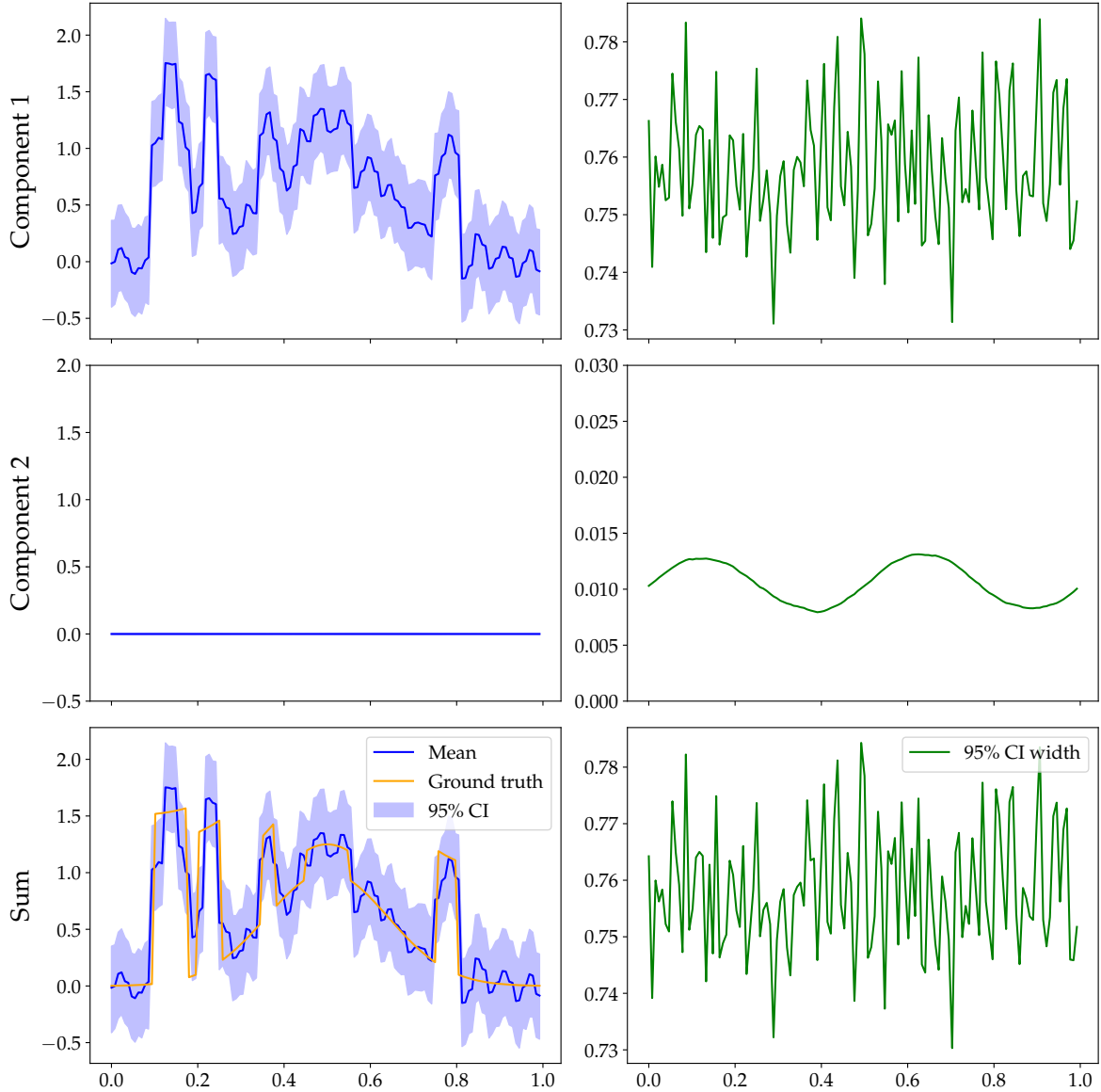


Figure 7: Posterior means and 95% CI widths from the hierarchical decomposition method with two Besov priors.

4.3. Image deblurring

In this section, we apply our hierarchical decomposition method proposed in Section 3 on a 2D deconvolution problem. We consider a separable Gaussian convolution kernel, i.e., the convolution is performed through a 1D Gaussian convolution defined in Section 4.1 along both the horizontal and vertical directions. The ground truth is the sum of a piecewise constant component and a smooth component. The resolution of \mathbf{f}_{true} is $n = 64^2 = 4096$, and the intensity range is $[0, 2]$. To generate the degraded data, we set $\sigma_{\text{ker}} = 1.0$ and the noise level 0.02. Figure 10 shows both the ground truth and the degraded image.

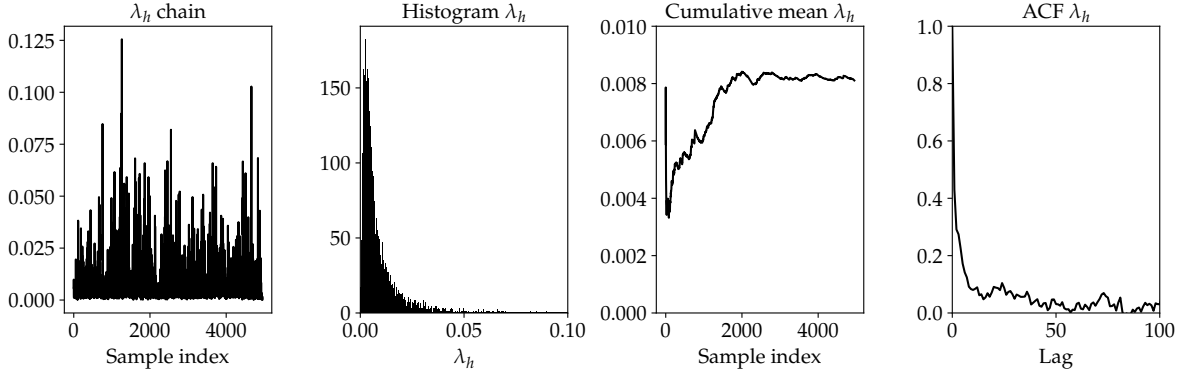


Figure 8: The posterior of the hyperparameter λ_h in the hierarchical decomposition method proposed in Section 3.

In our method, we use the DB(8) wavelet with $s_h = 3$ in the Besov prior for ψ_h . The parameters in the hyperpriors are set as $\alpha_1 = 1$, $\alpha_2 = 2$, $\beta_1 = 10^{-5}$ and $\beta_2 = 10^{-2}$. We run Algorithm 1 to generate 200 000 samples, from which we discard the first 10 000 as burn-in and thin the remaining samples by a factor of 30, providing 6334 samples used for analysis.

Figure 11 shows the posterior statistics for the hyperparameter λ_h . The chain appears well-mixed, the cumulative mean converges quickly, and the autocorrelation is low, indicating that the samples are reliable for posterior inference. In Figure 12 we show the posterior mean and the pixel-wise 95% CI width. The posterior mean of \mathbf{g} accurately captures the piecewise constant structure, and the posterior mean of \mathbf{h} reflects the smooth variations. According to the colorbar we can see that a part of the piecewise constant component was decomposed to \mathbf{h} , which indicates that an even smoother prior would be preferred for \mathbf{h} . Nevertheless, the posterior mean of \mathbf{f} is close to the ground truth with correct intensity range and the relative error of 0.06.

In the uncertainty plots of both \mathbf{h} and \mathbf{f} in Figure 12, we observe a regular, periodic pattern induced by the Besov prior. This structure is a natural consequence of the prior’s construction: when the Besov smoothness parameter $s_h \neq 0$, the scaling matrix \mathbf{S}_h is no longer a scalar multiple of the identity. Instead, it introduces scale-dependent weights, which result in anisotropic uncertainty. Such patterns are inherent to any non-trivial Besov prior and may appear more clearly in two-dimensional problems. In one dimension, or in problems where the likelihood dominates the prior, the effect may go unnoticed. A more detailed explanation is provided in Appendix B. However, ignoring these structural patterns, we still see that the higher uncertainties are mainly on the boundary of the object in \mathbf{f} .

Figure 13 shows the posterior means and the pixel-wise standard deviations (STDs) of the main diagonal in $\mathbf{\Lambda}$, which correspond to STDs of the first order derivatives of \mathbf{g} . It is clear that the posterior means are significant only near the boundaries, resulting in a sparse structure. These boundary regions also correspond to areas with noticeable

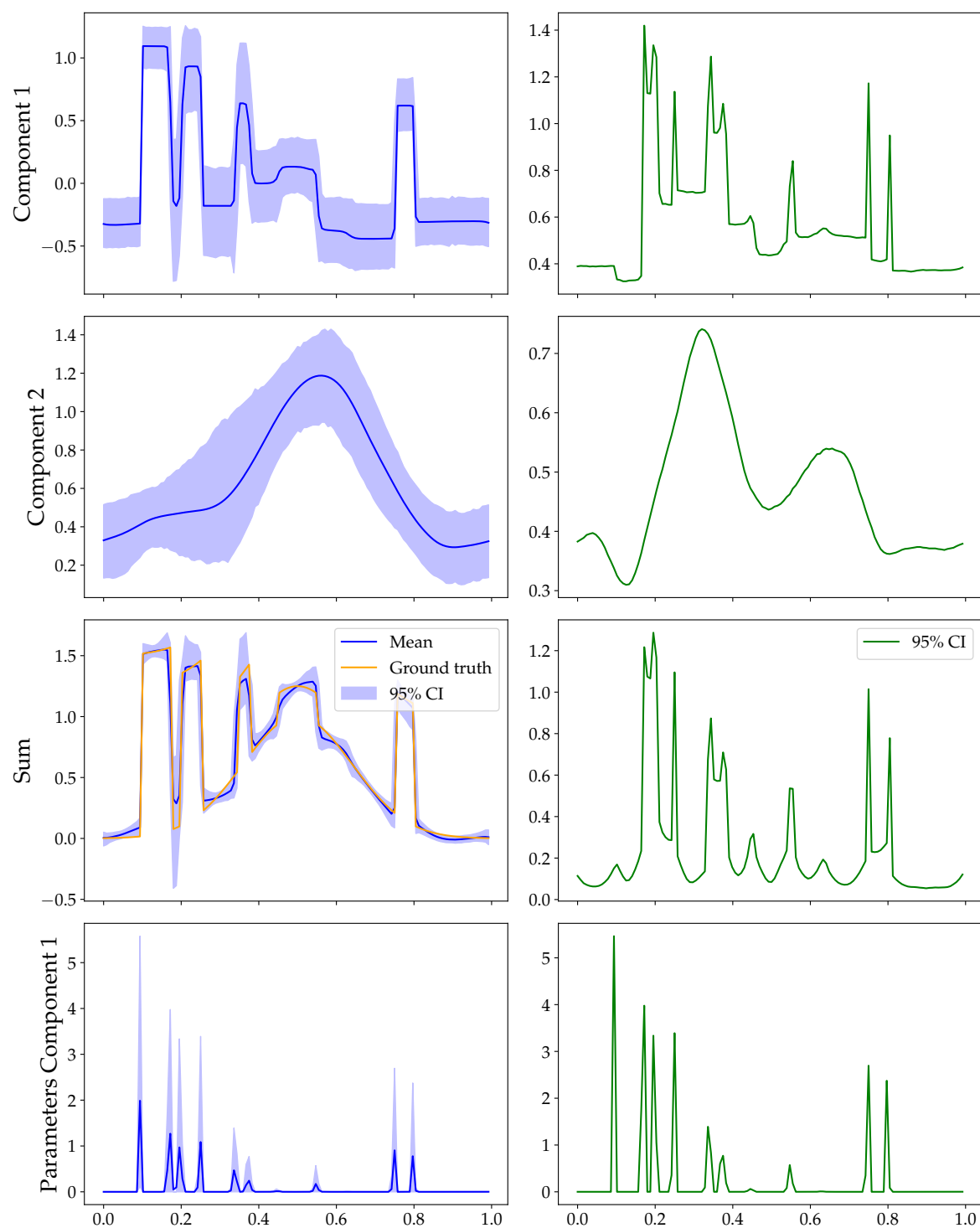


Figure 9: Posterior means and 95% CI widths in the hierarchical decomposition method introduced in Section 3.

high uncertainties.

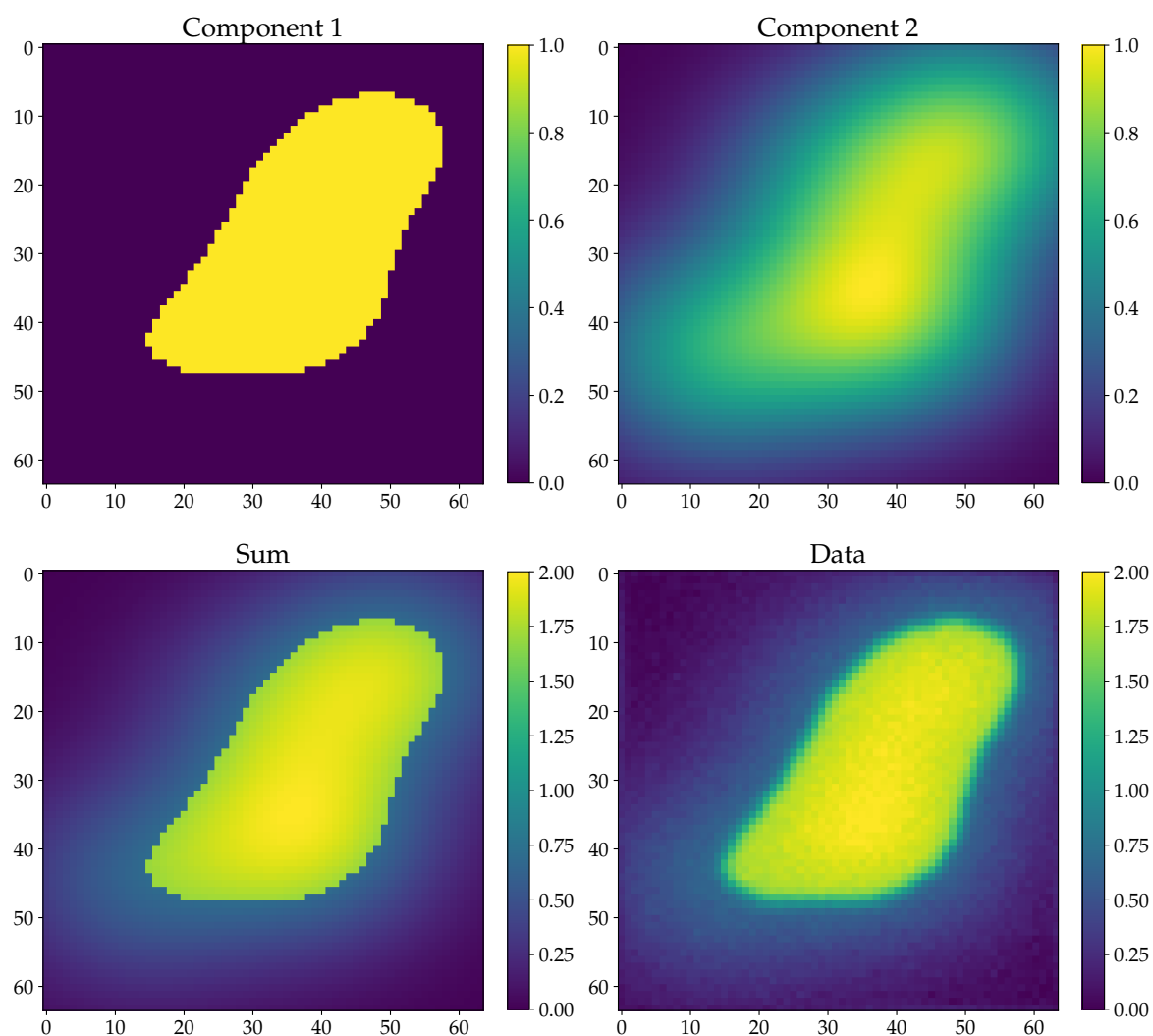


Figure 10: Ground truth and degraded image for the 2D deconvolution problem.

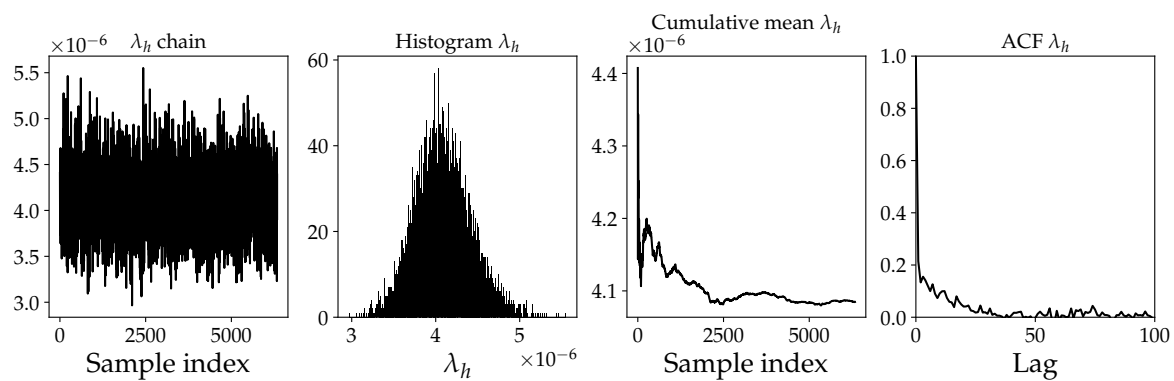


Figure 11: Posterior statistics of the hyperparameter λ_h from the hierarchical decomposition method for the 2D deconvolution problem.

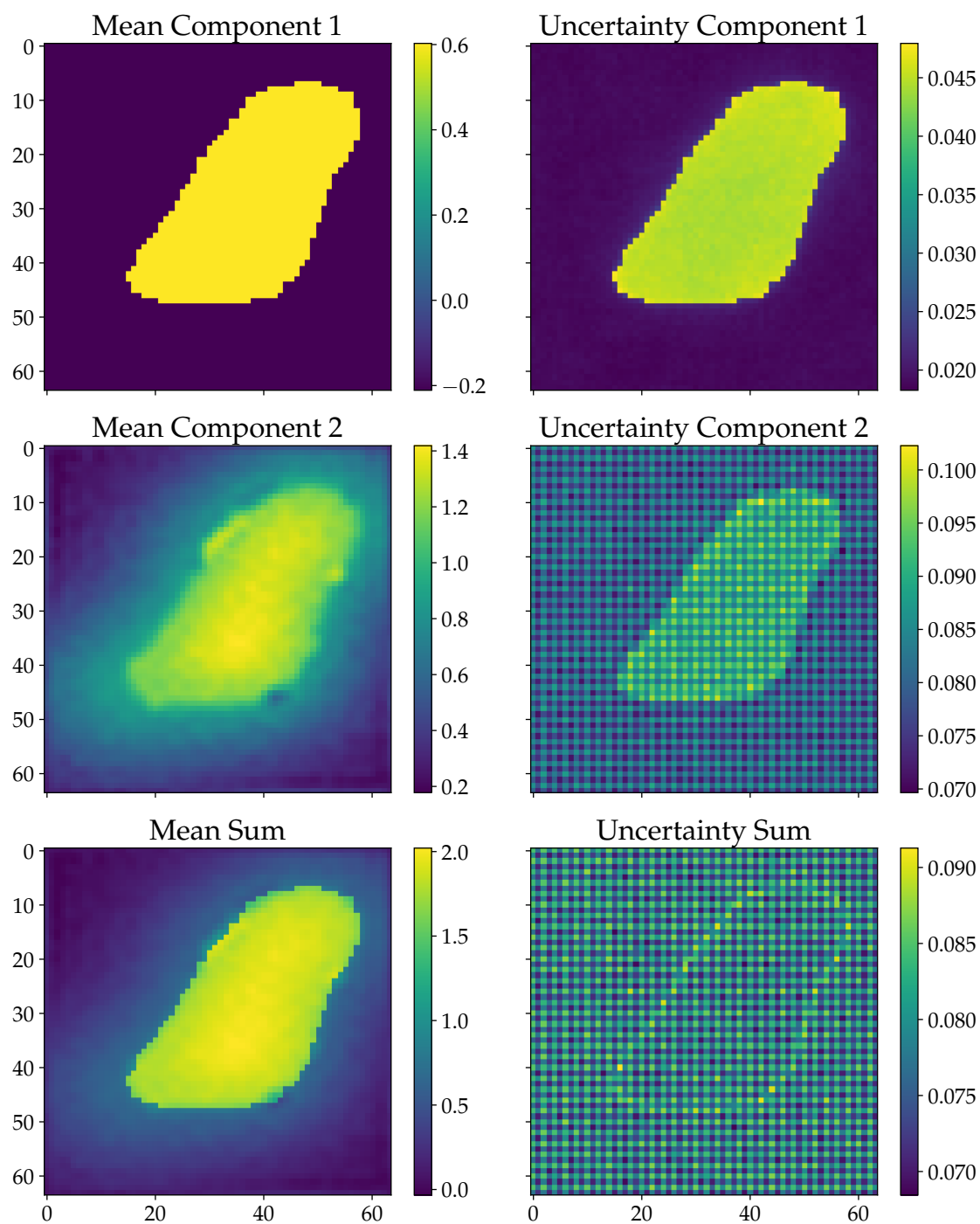


Figure 12: Posterior means and the pixel-wise 95% CI widths of \mathbf{g} , \mathbf{h} and \mathbf{f} for the 2D deconvolution problem.

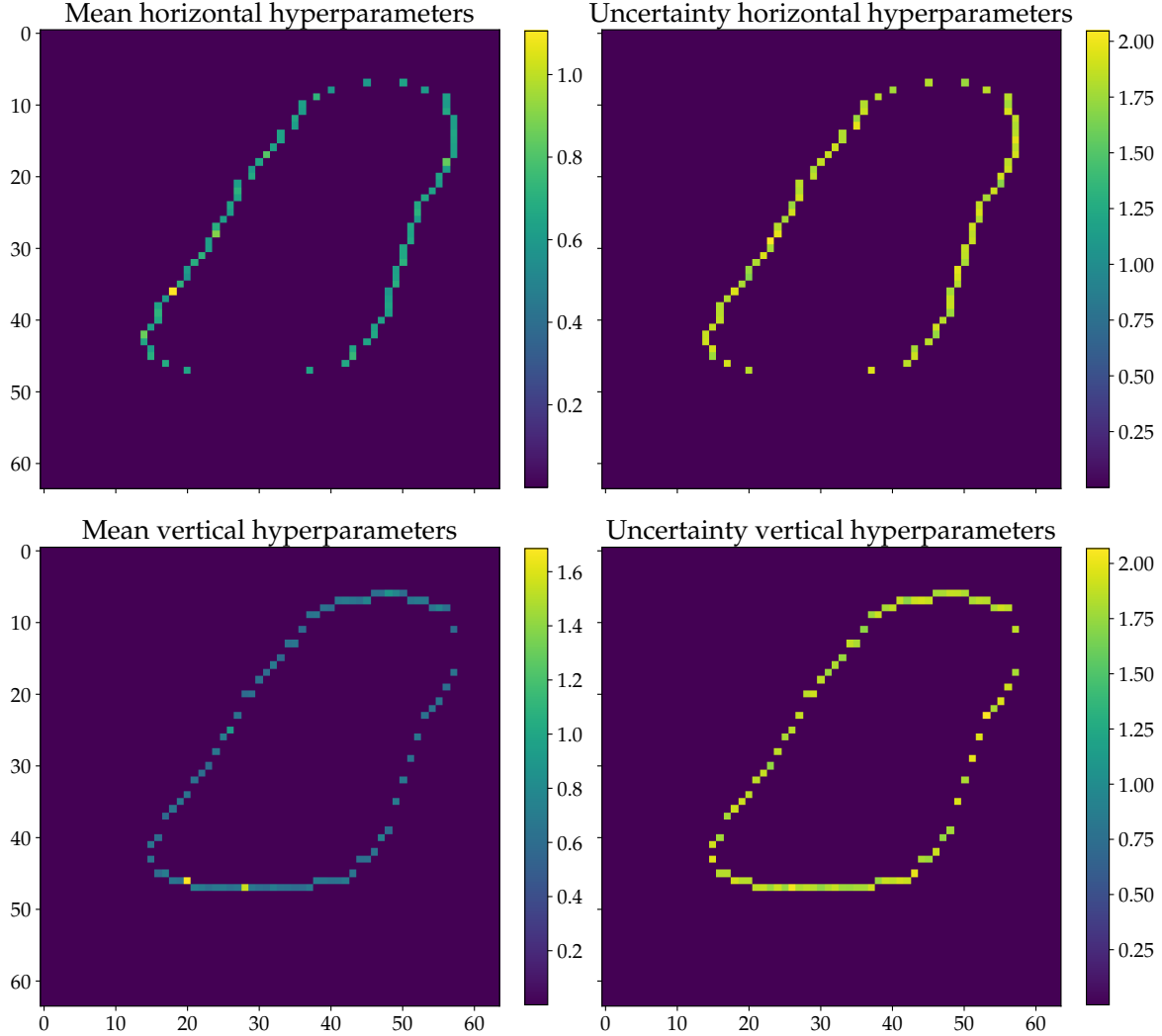


Figure 13: Posterior statistics of the hyperparameter Λ for the 2D deconvolution problem. Row 1: pixel-wise mean and STDs associated to horizontal derivative. Row 2: pixel-wise mean and STDs associated to vertical derivative.

5. Conclusion

In this paper, we have developed computational methods for solving linear Bayesian inverse problems where the unknown consists of smooth regions connected by localized jumps. Our approach is based on modeling the unknown as a sum of two components that individually describes either the smooth part or the jumps represented by a piecewise constant component. We propose two prior models that assign different priors to each component: the first combines two Besov priors, while the second uses a hierarchical Gaussian prior for the piecewise constant component and a smooth Besov prior for the smooth part.

We also address the challenge of selecting suitable hyperparameters for each prior

to ensure a balanced decomposition where both components contribute as desired. We use a hierarchical Bayesian approach and put hyperpriors on the parameters, and we propose a Gibbs sampling framework to infer the resulting posterior distribution.

From numerical experiments on 1D and 2D deconvolution problems, we conclude the following:

- The two-Besov prior model yields better reconstructions compared to a single Besov prior model, but sampling using NUTS results in more correlated posterior samples.
- In the two-Besov model, the balance between components is highly sensitive to the prior strength parameters.
- The hierarchical model with two Besov priors estimates the components and the prior strength parameters simultaneously. However, because of the identification issue, it often results in one component dominating the other, leading to unbalanced reconstructions.
- The hierarchical Gaussian-Besov decomposition model finds a parameter setting that achieves a balanced solution but with high correlation between the samples.

Acknowledgments

This work was supported by the Villum Investigator Grant (no. 25893) from the Villum Foundation. Babak Maboudi Afkham is partially supported by the Research Council of Finland project numbers: 359186, 353093.

Appendix A. Gibbs sampler for the hierarchical decomposition model with two Besov priors

We here consider a hierarchical formulation in which the prior strength parameters λ_g and λ_h in (19) are treated as random variables with associated hyperpriors. This approach follows the same Bayesian framework as the model in Section 3. However, it suffers from identifiability issues which can lead to imbalanced decompositions, where one component dominates. We include the sampling scheme here for completeness and comparison.

We assume that both λ_g and λ_h follow Gamma distributions defined as

$$\pi_{\text{hyp}}(\lambda_g) \propto \lambda_g^{a_1-1} \exp(-b_1 \lambda_g), \quad \pi_{\text{hyp}}(\lambda_h) \propto \lambda_h^{a_2-1} \exp(-b_2 \lambda_h), \quad (\text{A.1})$$

where a_1, b_1, a_2 and b_2 are all positive. Then the joint posterior on the components and hyperparameters is

$$\begin{aligned} \pi_{\text{post}}(\mathbf{g}, \mathbf{h}, \lambda_g, \lambda_h | \mathbf{y} = \mathbf{y}^*) &\propto \pi_{\text{like}}(\mathbf{y} = \mathbf{y}^* | \mathbf{g}, \mathbf{h}) \pi_{\text{prior}}(\mathbf{g} | \lambda_g) \pi_{\text{prior}}(\mathbf{h} | \lambda_h) \pi_{\text{hyp}}(\lambda_g) \pi_{\text{hyp}}(\lambda_h) \\ &\propto \lambda_g^{n/p_g+a_1-1} \lambda_h^{n/p_h+a_2-1} \exp\left(-\frac{1}{2\sigma^2} \|\mathbf{A}(\mathbf{g} + \mathbf{h}) - \mathbf{y}^*\|_2^2\right) \\ &\quad - \lambda_g \|\mathbf{S}_g \mathbf{W}_{\psi_g} \mathbf{g}\|_{p_g}^{p_g} - \lambda_h \|\mathbf{S}_h \mathbf{W}_{\psi_h} \mathbf{h}\|_{p_h}^{p_h} - b_1 \lambda_g - b_2 \lambda_h. \end{aligned} \quad (\text{A.2})$$

The posterior in (A.2) can be sampled using a similar Gibbs sampling method as in Algorithm 1 on four marginal distributions:

$$\pi_1(\mathbf{g}|\mathbf{y}^*, \lambda_g, \mathbf{h}) \propto \exp\left(-\frac{1}{2\sigma^2}\|\mathbf{A}(\mathbf{g} + \mathbf{h}) - \mathbf{y}^*\|_2^2 - \lambda_g\|\mathbf{S}_g\mathbf{W}_{\psi_g}\mathbf{g}\|_{p_g}^{p_g}\right) \quad (\text{A.3a})$$

$$\pi_2(\mathbf{h}|\mathbf{y}^*, \lambda_h, \mathbf{g}) \propto \exp\left(-\frac{1}{2\sigma^2}\|\mathbf{A}(\mathbf{g} + \mathbf{h}) - \mathbf{y}^*\|_2^2 - \lambda_h\|\mathbf{S}_h\mathbf{W}_{\psi_h}\mathbf{h}\|_{p_h}^{p_h}\right) \quad (\text{A.3b})$$

$$\pi_3(\lambda_g|\mathbf{g}) \propto \lambda_g^{n/p_g+a_1-1} \exp\left(-\lambda_g\|\mathbf{S}_g\mathbf{W}_{\psi_g}\mathbf{g}\|_{p_g}^{p_g} - b_1\lambda_g\right) \quad (\text{A.3c})$$

$$\pi_4(\lambda_h|\mathbf{h}) \propto \lambda_h^{n/p_h+a_2-1} \exp\left(-\lambda_h\|\mathbf{S}_h\mathbf{W}_{\psi_h}\mathbf{h}\|_{p_h}^{p_h} - b_2\lambda_h\right) \quad (\text{A.3d})$$

We set $p_g = p_h = 2$ and use RTO to sample π_1 and π_2 . The marginal distributions π_3 and π_4 can be sampled directly according to Gamma distributions defined as follows

$$\lambda_g^{\text{sample}} \sim \mathcal{G}(a_1 + n/2, b_1 + \|\mathbf{S}_g\mathbf{W}_{\psi_g}\mathbf{g}\|_2^2), \quad (\text{A.4a})$$

$$\lambda_h^{\text{sample}} \sim \mathcal{G}(a_2 + n/2, b_2 + \|\mathbf{S}_h\mathbf{W}_{\psi_h}\mathbf{h}\|_2^2). \quad (\text{A.4b})$$

Appendix B. Anisotropic uncertainty in Besov priors

We consider the case where the wavelet coefficients $\mathbf{c} \in \mathbb{R}^n$ are drawn from a product distribution of identically distributed generalized Gaussian random variables with density (9). The Besov prior is defined through the wavelet expansion (11), and the reconstructed signal is $\mathbf{f} = \mathbf{B}\mathbf{c}$, where $\mathbf{B} = \mathbf{W}_{\psi}^T\mathbf{S}^{-1}$ combines the inverse wavelet transform \mathbf{W}_{ψ}^T and the diagonal Besov scaling matrix \mathbf{S}^{-1} from (14) and (13), respectively.

Since \mathbf{c} has a smooth, strictly positive density and \mathbf{B} is invertible, the distribution of \mathbf{f} is absolutely continuous and given by the pushforward measure

$$\mu_f = \mathbf{B}_{\#}\mu_c,$$

where μ_c is the product measure on \mathbb{R}^n . While c_i for $i = 1, \dots, n$ are independent, the components of $\mathbf{f} = \mathbf{B}\mathbf{c}$ are dependent, and the distribution of \mathbf{f} is no longer product-structured or generalized Gaussian. For $p = 2$, $\mathbf{c} \sim N(0, \sigma_p^2 I)$ implies $\mathbf{f} \sim N(0, \sigma_p^2 \mathbf{B}\mathbf{B}^T)$, but for $p \neq 2$, no closed-form density exists.

The distribution of \mathbf{f} remains symmetric about the origin, with marginal tails still governed by p . The covariance matrix of \mathbf{f} is given by

$$\text{cov}(\mathbf{f}) = \mathbf{B} \text{cov}(\mathbf{c}) \mathbf{B}^T = \sigma_p^2 \mathbf{B}\mathbf{B}^T.$$

In Besov priors, where $\mathbf{B} = \mathbf{W}_{\psi}^T\mathbf{S}^{-1}$, this becomes

$$\text{cov}(\mathbf{f}) = \sigma_p^2 \mathbf{W}_{\psi}^T \mathbf{S}^{-2} \mathbf{W}_{\psi}. \quad (\text{B.1})$$

This covariance matrix is not a multiple of the identity unless $s + d/2 - d/p = 0$ and the wavelet transform is orthonormal, i.e., bi-orthogonal wavelets *or* non-trivial Besov weights will lead to anisotropic covariance.

It is the dyadic structure of \mathbf{S} that disrupts the perfect reconstruction property of the wavelet transform and gives rise to a structured variation in the standard deviation of the samples, which can be interpreted as artifacts or patterns in the prior samples. The structured patterns, illustrated in our numerical experiments, are due to upsampling in the inverse wavelet transform, variation of the wavelet filter, and scale-dependent weighting. The resulting uncertainty patterns in posterior estimates, such as pointwise confidence intervals, arise from this anisotropic covariance structure.

References

- [1] Antonin Chambolle and Pierre-Louis Lions. Image recovery via total variation minimization and related problems. *Numerische Mathematik*, 76(2):167–188, 1997.
- [2] Jean-Luc Starck, Michael Elad, and David L. Donoho. Image decomposition via the combination of sparse representations and a variational approach. *IEEE Transactions on Image Processing*, 14(10):1570–1582, 2005.
- [3] Yiming Gao and Xiaoping Yang. Infimal convolution type regularization of TGV and shearlet transform for image restoration. *Computer Vision and Image Understanding*, 182:38–49, 2019.
- [4] Zhiyuan Zhang and Hongjin He. A customized low-rank prior model for structured cartoon–texture image decomposition. *Signal Processing: Image Communication*, 96:116308, 2021.
- [5] Baoshun Shi, Chunzi Zhu, Lingyan Li, and Huagui Huang. Cartoon-texture guided network for low-light image enhancement. *Digital Signal Processing*, 144:104271, 2024.
- [6] Jari P. Kaipio and Erkki Somersalo. Estimating anomalies from indirect observations. *Journal of Computational Physics*, 181(2):398–406, 2002.
- [7] Daniela Calvetti and Erkki Somersalo. *Subjective Knowledge or Objective Belief? An Oblique Look to Bayesian Methods*, chapter 3, pages 33–70. John Wiley & Sons, Ltd, 2010.
- [8] Julianne Chung, Jiahua Jiang, Scot M. Miller, and Arvind K. Saibaba. Hybrid projection methods for solution decomposition in large-scale Bayesian inverse problems. *SIAM Journal on Scientific Computing*, 46(2):S97–S119, 2024.
- [9] Daniela Calvetti, Laura Homa, and Erkki Somersalo. Bayesian mixture models for source separation in MEG. *Inverse Problems*, 27(11):115001, oct 2011.
- [10] Silja L Christensen, Nicolai A B Riis, Marcelo Pereyra, and Jakob S Jørgensen. A Bayesian approach for CT reconstruction with defect detection for subsea pipelines. *Inverse Problems*, 40(2):025003, dec 2023.
- [11] Gitta Kutyniok and Wang-Q Lim. Image separation using wavelets and shearlets. In Jean-Daniel Boissonnat, Patrick Chenin, Albert Cohen, Christian Gout, Tom Lyche, Marie-Laurence Mazure, and Larry Schumaker, editors, *Curves and Surfaces*, pages 416–430, Berlin, Heidelberg, 2012. Springer Berlin Heidelberg.
- [12] Jerome Bobin, Jean-Luc Starck, Jalal M. Fadili, Yassir Moudden, and David L. Donoho. Morphological component analysis: An adaptive thresholding strategy. *IEEE Transactions on Image Processing*, 16(11):2675–2681, 2007.
- [13] Rémi. Gribonval and Emmanuel Bacry. Harmonic decomposition of audio signals with matching pursuit. *IEEE Transactions on Signal Processing*, 51(1):101–111, 2003.
- [14] Yu Liu, Xun Chen, Rabab K. Ward, and Z. Jane Wang. Medical image fusion via convolutional sparsity based morphological component analysis. *IEEE Signal Processing Letters*, 26(3):485–489, 2019.
- [15] Erkki Somersalo Jari P. Kaipio. *Statistical and Computational Inverse Problems*. Springer-Verlag, New York, 2005.
- [16] Masoumeh Dashti and Andrew M. Stuart. *The Bayesian Approach to Inverse Problems*, pages 311–428. Springer International Publishing, Cham, 2017.

- [17] Iain Henderson. Sobolev regularity of Gaussian random fields. *Journal of Functional Analysis*, 286(3):110241, 2024.
- [18] Matti Lassas, Eero Saksman, and Samuli Siltanen. Discretization-invariant Bayesian inversion and Besov space priors. *Inverse Problems and Imaging*, 3(1):87–122, 2009.
- [19] Masoumeh Dashti, Stephen Harris, and Andrew Stuart. Besov priors for Bayesian inverse problems. *Inverse Problems and Imaging*, 6(2):183–200, 2012.
- [20] Jarkko Suuronen, Neil K Chada, and Lassi Roininen. Cauchy Markov random field priors for Bayesian inversion. *Statistics and computing*, 32(2):33, 2022.
- [21] Jarkko Suuronen, Tomás Soto, Neil K Chada, and Lassi Roininen. Bayesian inversion with α -stable priors. *Inverse Problems*, 39(10):105007, 2023.
- [22] Felipe Uribe, Johnathan M Bardsley, Yiqiu Dong, Per Christian Hansen, and Nicolai AB Riis. A hybrid Gibbs sampler for edge-preserving tomographic reconstruction with uncertain view angles. *SIAM Journal on Uncertainty Quantification*, 10(3):1293–1320, 2022.
- [23] Angelina Senchukova, Felipe Uribe, and Lassi Roininen. Bayesian inversion with Student’s t priors based on Gaussian scale mixtures. *Inverse Problems*, 40(10):105013, sep 2024.
- [24] Rafael Flock, Yiqiu Dong, Felipe Uribe, and Olivier Zahm. Certified coordinate selection for high-dimensional Bayesian inversion with Laplace prior. *Statistics and Computing*, 34(4):134, 2024.
- [25] Daniela Calvetti, Erkki Somersalo, and Alexander Strang. Hierarchical Bayesian models and sparsity: ℓ_2 -magic. *Inverse Problems*, 35(3):035003, 2019.
- [26] Felipe Uribe, Yiqiu Dong, and Per Christian Hansen. Horseshoe priors for edge-preserving linear Bayesian inversion. *SIAM Journal on Scientific Computing*, 45(3):B337–B365, 2023.
- [27] Daniela Calvetti, Monica Pragliola, and Erkki Somersalo. Sparsity promoting hybrid solvers for hierarchical bayesian inverse problems. *SIAM Journal on Scientific Computing*, 42(6):A3761–A3784, 2020.
- [28] Yiqiu Dong and Monica Pragliola. Inducing sparsity via the horseshoe prior in imaging problems. *Inverse Problems*, 39(7):074001, jun 2023.
- [29] Nathan Waniorek, Daniela Calvetti, and Erkki Somersalo. Bayesian hierarchical dictionary learning. *Inverse Problems*, 39(2):024006, feb 2023.
- [30] Chen Li, Matthew Dunlop, and Georg Stadler. Bayesian neural network priors for edge-preserving inversion. *Inverse Problems and Imaging*, 16(5):1229–1254, 2022.
- [31] Jan Glaubitz and Anne Gelb. Leveraging joint sparsity in hierarchical Bayesian learning. *SIAM/ASA Journal on Uncertainty Quantification*, 12(2):442–472, 2024.
- [32] Rémi Laumont, Valentin De Bortoli, Andrés Almansa, Julie Delon, Alain Durmus, and Marcelo Pereyra. Bayesian imaging using plug & play priors: When Langevin meets Tweedie. *SIAM Journal on Imaging Sciences*, 15(2):701–737, 2022.
- [33] Hanne Kekkonen, Matti Lassas, Eero Saksman, and Samuli Siltanen. Random tree Besov priors—towards fractal imaging. *Inverse Problems and Imaging*, 17(2), 2023.
- [34] Keijo Hämäläinen, Aki Kallonen, Ville Kolehmainen, Matti Lassas, Kati Niinimäki, and Samuli Siltanen. Sparse tomography. *SIAM Journal on Scientific Computing*, 35(3):B644–B665, 2013.
- [35] Ville Kolehmainen, Matti Lassas, Kati Niinimäki, and Samuli Siltanen. Sparsity-promoting Bayesian inversion. *Inverse Problems*, 28(2):025005, 1 2012.
- [36] Andreas Horst, Babak Maboudi Afkham, Yiqiu Dong, and Jakob Lemvig. Uncertainty quantification for linear inverse problems with Besov prior: A randomize-then-optimize method. *Statistics and Computing*, 35(101), 2025.
- [37] Matthew D. Hoffman and Andrew Gelman. The No-U-Turn Sampler: Adaptively setting path lengths in Hamiltonian Monte Carlo. *Journal of Machine Learning Research*, 15(47):1593–1623, 2014.
- [38] Johnathan M. Bardsley, Antti Solonen, Heikki Haario, and Marko Laine. Randomize-then-optimize: A method for sampling from posterior distributions in nonlinear inverse problems. *SIAM Journal on Scientific Computing*, 36(4):A1895–A1910, 2014.

- [39] Christoph Schwab and Andreas Stein. Multilevel Monte Carlo FEM for elliptic PDEs with Besov random tree priors. *Stochastics and Partial Differential Equations: Analysis and Computations*, 12(3):1574–1627, 2024.
- [40] Ingrid Daubechies. Orthonormal bases of compactly supported wavelets. *Communications on Pure and Applied Mathematics*, 41(7):909–996, 1988.
- [41] Stéphane Mallat. *A wavelet tour of signal processing*. Elsevier, 1999.
- [42] Hans Triebel. *Function Spaces and Wavelets on Domains*. European Mathematical Society, Zürich, 2008.
- [43] Hans Triebel. *Theory of Function Spaces III*. Birkhäuser, Basel, 01 2006.
- [44] Stéphane G. Mallat. A theory for multiresolution signal decomposition: The wavelet representation. *IEEE Trans. Pattern Anal. Mach. Intell.*, 11(7):674–693, 1989.
- [45] Gregory R. Lee, Ralf Gommers, Filip Waselewski, Kai Wohlfahrt, and Aaron O’Leary. Pywavelets: A Python package for wavelet analysis. *Journal of Open Source Software*, 4(36):1237, 2019.
- [46] David L. Donoho and Michael Elad. Optimally sparse representation in general (nonorthogonal) dictionaries via l^1 minimization. *Proc. Natl. Acad. Sci. USA*, 100(5):2197–2202, 2003.
- [47] Magnus R Hestenes, Eduard Stiefel, et al. Methods of conjugate gradients for solving linear systems. *Journal of research of the National Bureau of Standards*, 49(6):409–436, 1952.